2006

Rapid Prototyping Of Microfluidic Packages

Michael Pepper
University of Central Florida

RAPID PROTOTYPING OF MICROFLUIDIC PACKAGES

by

MICHAEL R. PEPPER
B.S. University of Central Florida, 2002

A thesis submitted in partial fulfillment of the requirements
for the degree of Master of Science
in the Department of Mechanical Materials and Aerospace Engineering
in the College of Engineering and Computer Science
at the University of Central Florida
Orlando, Florida

Spring Term
2006

ABSTRACT

In the area of MEMS there exists a tremendous need for communication between the micro-device and the macro world. A standard protocol or at least multiple standards would be of great use. Electrical connections have been standardized for many uses and configurations by the integrated circuit industry. Standardization in the IC industry has created a marketplace for digital devices unprecedented. In addition to the number of "off the shelf" products available, there exists the possibility for consumers to mix and match many devices from many different manufacturers. This research proposes some similar solutions as those for integrated circuits for fluid connections and mechanical configurations that could be used on many different devices. In conjunction with offering the capability to facilitate communication between the micro and macro worlds, the packaging solutions should be easy to fabricate. Many devices are by nature non-standard, unique, designs that make a general solution difficult. At the same time, the micro-devices themselves will inevitably need to evolve some standardization.

In BioMEMS devices the packaging issue is concerned with delivering a sample to the device, conducting the sample to the sensor or sensors, and removing the sample. Conducting the sample to the sensor or sensors is usually done with microchannels created by standard MEMS fabrication techniques. Many current designs then utilize conventional machining techniques to create the inlet and outlet for the sample. This work proposes a rapid prototyping method for creating the microchannel and inlet / outlet in simplified steps. The packages developed from this process proved to be an effective solution for many applications.

ACKNOWLEDGMENTS

I would like to take this opportunity to thank first my advisor, Dr. Hyoung J. Cho for his guidance and his giving me the opportunity to work under and learn from him. The experience that I have gained through being a part of the Nanofab and BioMEMS lab is invaluable. I would like to thank Dr. Ted Conway for getting me involved in the Master's program. The field of engineering research would be completely unknown to me if not for these men.

I would like to thank Dr. Samar Kalita and Dr Xun Gong for agreeing to be on my thesis committee. I would like to thank Dr Quanfang Chen and Dr. Samar Kalita for their advise, knowledge, and laboratory time. I would like to acknowledge the committee members, Dr. Hyoung J. Cho, Dr Samar Kalita, and Dr. Xun Gong.

I would like to thank all my friends and colleagues in the NanoFab and BioMEMS lab, Hyoungseok, Anjum, Naveen, Shyam, Andrea, Peng, and Joseph. A special thank you to Richard Zotti, a good man and a great machinist.

Of course and most importantly, thank you to my parents, my sister, my brother-in-law for the unconditional love and support throughout my life. I could not have done this without you.

TABLE OF CONTENTS

LIST OF FIGURES

LIST OF ACRONYMS/ABBREVIATIONS

COC	Cyclic Olefin Copolymer
ECDM	Electro-Chemical Discharge Machining
FEA	Finite Element Analysis
MEMS	Micro-Electro-Mechanical-Systems
PDMS	Polydimethylsiloxane
PMMA	Polymethylmethacrylate

CHAPTER ONE: INTRODUCTION

1.1 Background

MEMS (Micro-Electro-Mechanical-Systems) is an emerging area of technology that promises great advancements for many industries. The rapid reproduction of microstructures is one facet of MEMS that can assist in the development of these advances. Since MEMS technology is relatively new, many fabrication processes and industry standards are not yet fully realized. One of the technical challenges in this field is the lack of standardization. In addition, some of the designs are limited by deficiencies in established fabrication techniques. Although the great advantage of the MEMS process is its capability for batch production, in the design and prototyping stage, an adequate technique for small scale rapid prototyping is desired. In this work, a new method for rapid prototyping for MEMS packaging components was studied. This study involves the development of a procedure for rapidly, inexpensively, and dependably fabricating packaging solutions. Advances in the fabrication processes will shape the future design of biomedical, electronics, and aeronautics devices.

1.1.1 Rapid Prototyping for Microfluidic Devices

This research will present a new method for the rapid replication of microfluidic packages. Some previous research involving similar processes is described briefly below.

One of the most frequently adopted methods in generating features for microfluidic devices involve the use of a compliant and self-sealing material; polydimethylsiloxane (PDMS). One example can be found in Janelle R. Anderson et al's work [1]. They presented a fabrication process entitled as "membrane sandwich". This procedure involves molding microchannels into

each face of thin membranes in polydimethylsiloxane (PDMS) using a SU-8 template that is fabricated separately by photolithography. Next they created vias or holes that are connections between each face and then they sandwich these membranes (Figure 1) in between two flat slabs for structural support and enclosing the channels. Membranes of about 20 micrometers in thickness were created (Figure 2). The bond between the membranes and slabs was from the noncovalent interfacial adhesion. To seal the parts, the parts were oxidized in an air-plasma and then the faces were brought into contact with each other. (Figure 3) Starting from a master template, a very complex structure (Figure 4) can be made. However, the casting and assembly processes take time and labor. The substrate is limited to PDMS, which is not very suitable for scaled-up production.

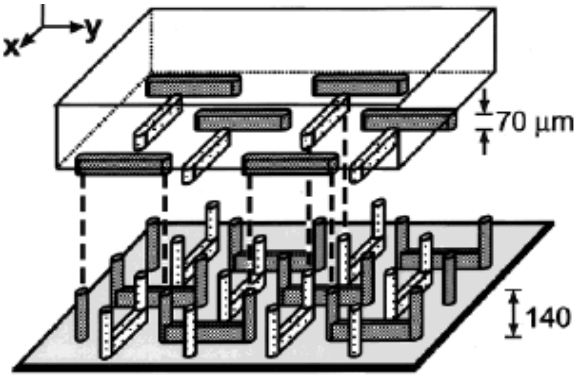

Figure 1. Schematic of upper and lower membrane with microchannels

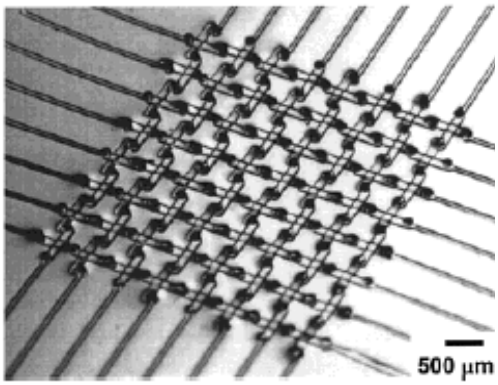

Figure 2. Optical micrograph of unenclosed lower membrane and microchannels in PDMS

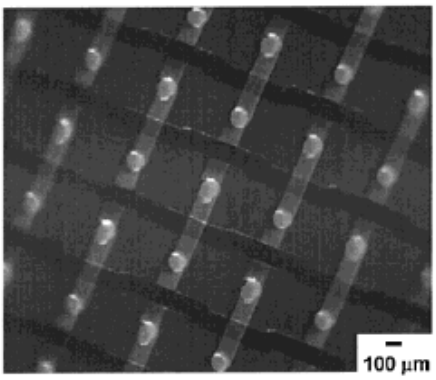

Figure 3. Optical micrograph of upper and lower membranes assembled with fluid in microchannels

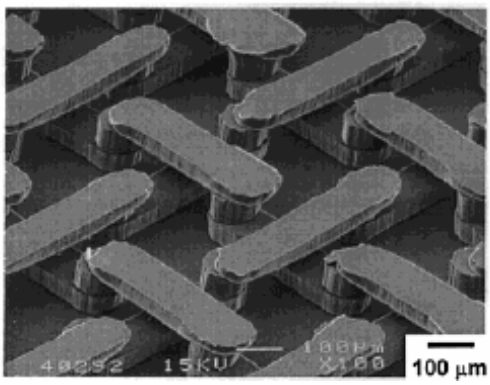

Figure 4. Optical micrograph of an epoxy casting from the microchannels. The microchannels were filled with epoxy and the PDMS was dissolved

Research similar to the "membrane sandwich" was studied by Bernhard H. Weigl et al [2]. Micronics, Inc used a stacking sandwich type configuration called ORCAμFluidic^{Tm} for their microfluidic device (Figure 5). The difference with their process lies in the fabrication of each level. They use a laser cutting system on an undisclosed polymer material to create the microchannels in each thin layer. Features and channels in the thin layers are cut all the way though the layer. Due to this technique, each thin layer requires a top cover and bottom cover (Figure 5). The channels are separated where desired by these covers, but where a connection between channels is needed there will be hole in the cover to connect the channels. All of the features are designed in AutoCAD and shaped from 11"x17" plastic sheet cut by a laser cutting machine similar to a plotter and pen setup. This method is a serial process which will prove to be time consuming and expensive.

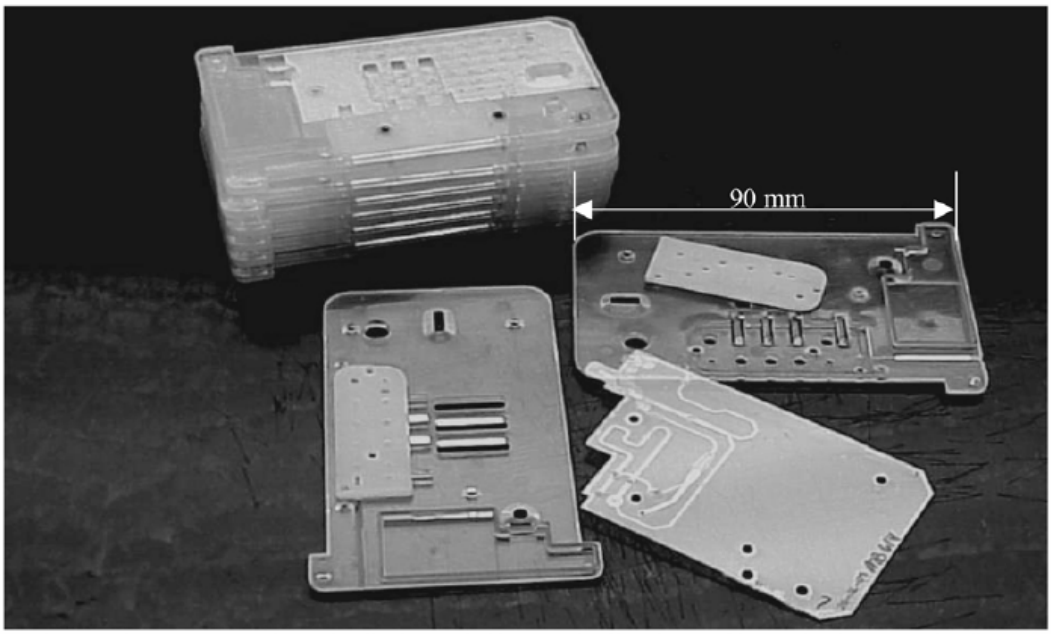

Figure 5. Micronic's hematology cartridge: Thin films and covers assembled [2]

Christophe Provin et al [3] presented research that entailed using a 3D solid object computer model in a stereolithography machine (Figure 6) to generate a 3D part of a geometry that is beyond the abilities of other fabrications (Figure 7,8). The basic idea of stereolithography is that of laser induced polymerization from a liquid bath to a solid object. The object is designed in 3D solid modeling software. The software then converts the single solid object into hundreds or thousands of 2D slices. These slices are built up successively in the liquid polymer by the laser solidification. All these slices stacked on top of each other make the 3D solid. Most processes like this use a polymer that is photoreactive but not very mechanically strong. In this particular case, the authors put a ceramic powder into the photocurable monomer. With the addition of the ceramic powder, a greater range of mechanical properties is available. Some post processes that would increase the mechanical properties of the finished part is also possible. For our purposes, the polymer that we use for stereolithography or for micro-injection molding has

the right mechanical properties. Although our mechanical testing reveals a higher operating strength with this fabrication process then with our fabrication process, the main concern for our designs is the property of being biologically inert. The mechanical strength is therefore often not the only driving factor.

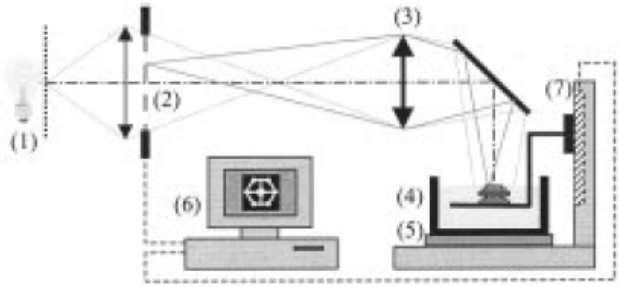

Figure 6. Schematic of stereolithography process: 1) high-pressure hg light 2) LCD 3) imaging system 4) photoreactor 5) temperature regulation 6) computer 7) vertical moving stage [4]

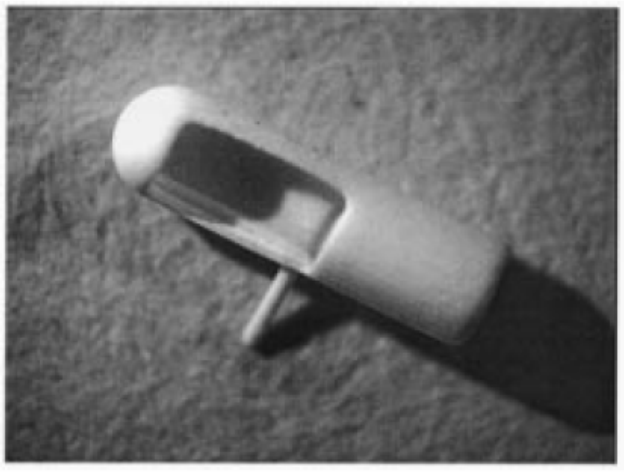

Figure 7. Pictures of ceramic-polymer microparts microcatheter tip[4]

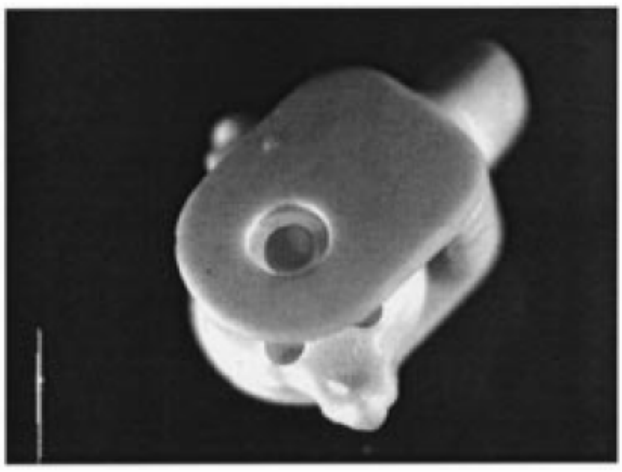

Figure 8. Pictures of ceramic-polymer microparts microgimball for micro robot [4]

Indalesio Rodriguez et al [3] presented two different rapid fabrication approaches for microchannels in glass. The first process involves patterning a microchannel arrangement on a PDMS face, sealing that face against the glass substrate, and passing an etchant through the channels (Figure 11). The etchant will attack the glass and not the PDMS, which will leave the microchannel arrangement in the glass. The second process investigated is a more conventional masking with electroplated nickel and etching. Comparing the two processes the group discovered that the nickel mask was generating a rectangular cross section (Figure 10) while the PDMS generated a parabolic cross section (Figure 9). Differences in the cross sections of the microchannels were due to the quality of the seal between the substrate and the mask. Accuracy is a problem with the PDMS masking as can be seen in the resultant cross section of the microchannel. The mechanism that produces the parabolic cross section, poor sealing between the PDMS and glass, will also cause issues with repeatability. A functioning microfluidic device can be made by simple microinjection molding in one step as opposed to the multiple steps presented in this research.

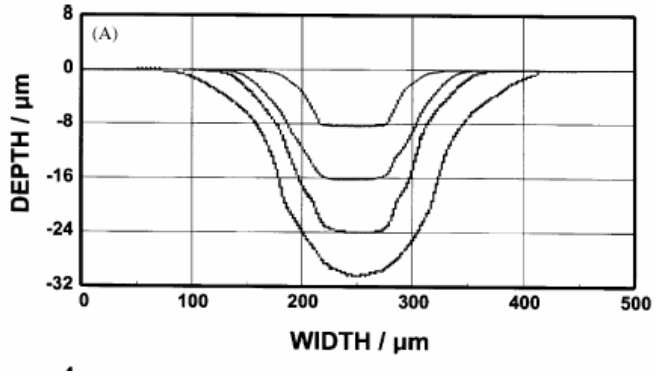

Figure 9. Cross-section with PDMS as mask

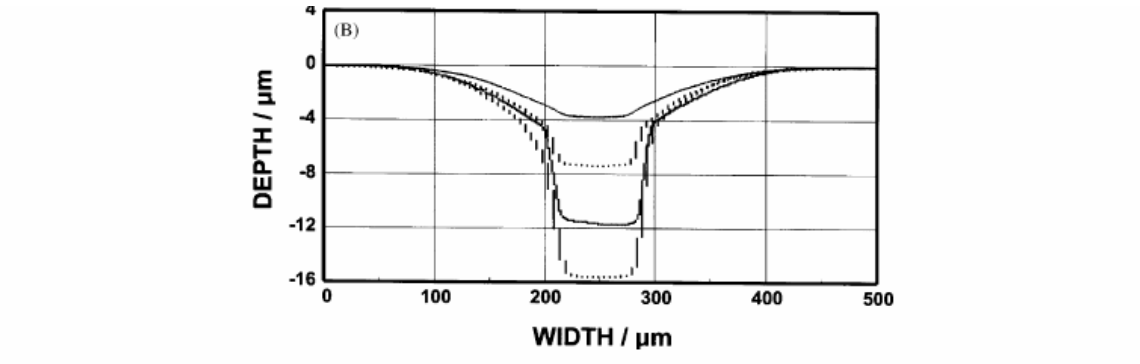

Figure 10. Cross-section of Ni as mask [3]

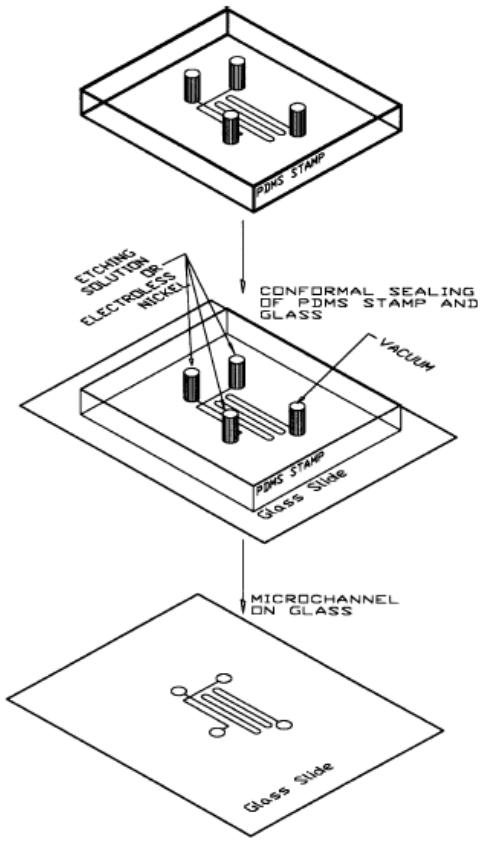

Figure 11. Schematic of PDMS mask, etch, and result [3]

Jagannathan Narasimhan et al [4] presented research work that involved a combination of rapid prototyping and hot embossing. The group first used a photolithography process with

AZ4620 or SU-8 photoresists to create a mold that will then be used to cast PDMS into a tool (Figure 12) that is the negative of the desired final part shape. The PDMS negative will be pressed into molten PMMA to generate the final part. The PDMS tool and PMMA thermoplastic were then heated together on a hot plate at a temperature above the glass transition temperature of the PMMA, but below the glass transition temperature of the PDMS, with a constant pressure. The system is then cooled with the force still applied until the temperature drops below the glass transition temperature of the PMMA. After this, the system is cooled to room temperature, the force is released, and the tool and part are separated. Remaining is a very accurate reproduction of the desired part (Figure 13, 14, 15). The deformation of the PDMS and its lifetime due to elastomeric characteristics could be areas of concern.

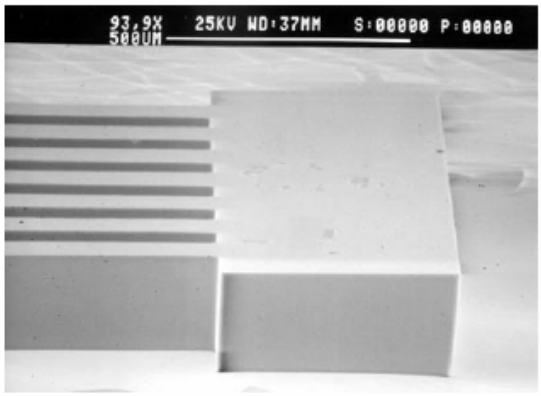

Figure 12. PDMS embossing tool [4]

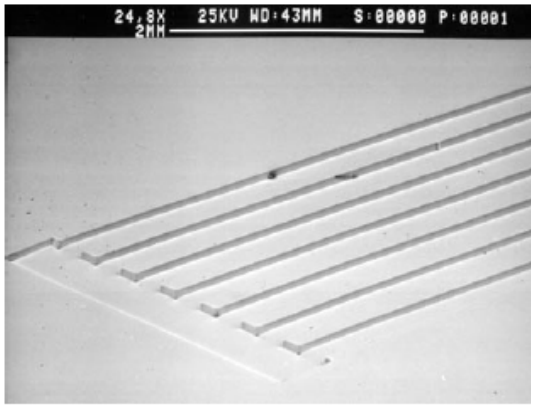

Figure 13. Embossed pattern in PMMA [4]

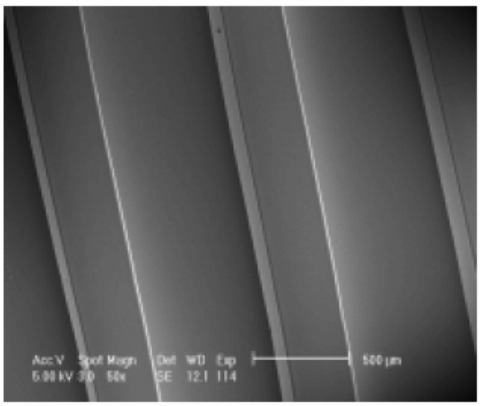

Figure 14. PMMA channels 250 µm deep [4]

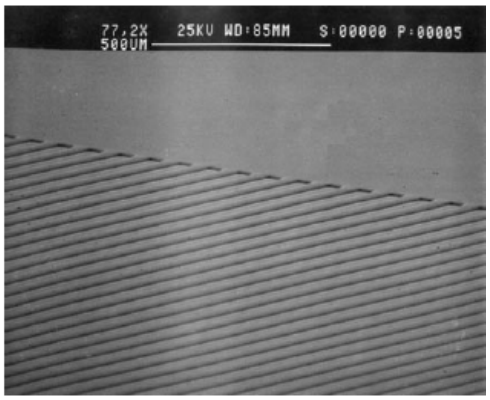

Figure 15. PMMA channels 5 µm deep [4]

1.1.2 Microfluidic Packaging and Interconnection

In 1998 C. Gonzalez et al [5] presented a modular system for microfluidic interconnections. There are two-parts to this system consisting of on-board interconnections and inlet/outlet interconnections. The first part of the system incorporates some “interlocking finger

joints" (Figure 16, 17) which are sets of similar grooves and teeth on two separate pieces. Each piece has microchannels fabricated in it and an O-ring or gasket is fabricated in one of the pieces. The interlocking force of these joints creates enough compression to generate an effective seal (Figure 17) and the geometry of the joints allows for good alignment. The second part of the system, the inlet/outlet interconnection, is composed of a hex-shaped two-piece silicon tube (Figure 18). The silicon tube is fabricated by etching channels into both sides of a (100) silicon substrate, creating a half hex, then etching a channel into the middle of the half hex. When two half hexes are bonded, the result is the hex-shaped silicon tube. Standard commercial tubing can be fitted to this silicon tube (Figure 19). This system requires manual machining for the joints, photolithography for the microfluidic channels, photolithography for the O-ring gasket, photolithography for the silicon tubes, and then manual assembly. The packages presented in my current research are fabricated by one process each respectively: microinjection molding (type I), stereolithography (type II), and conventional machining (type III).

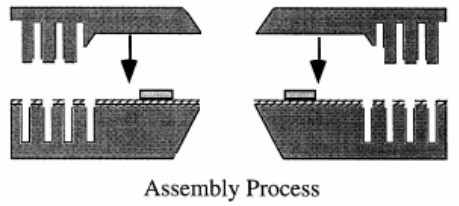

Figure 16. Interlocking finger joints with gasket [5]

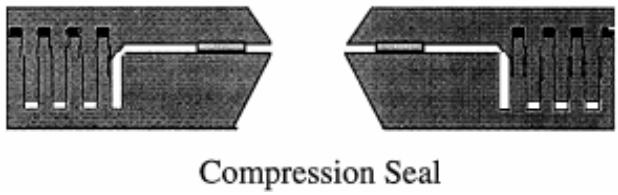

Figure 17. Interlocking finger joints with gasket closed [5]

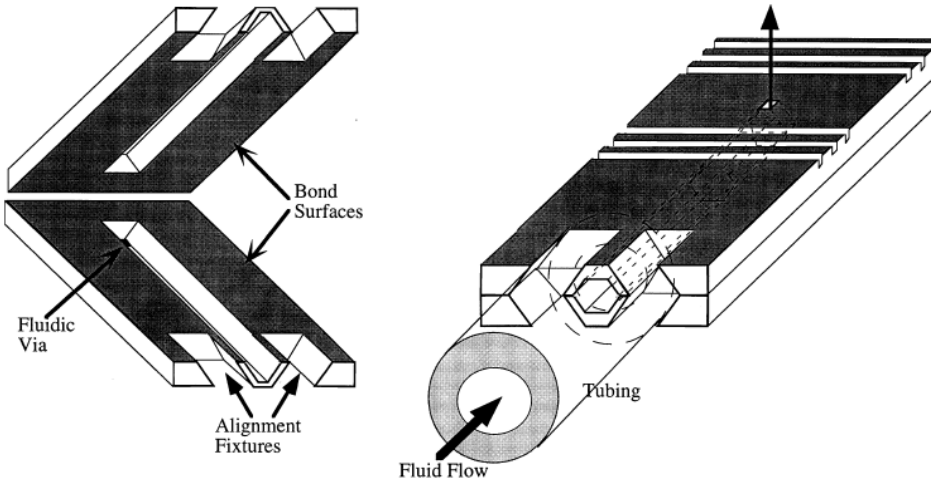

Figure 18. Inlet/outlet interconnection with tubing [5]

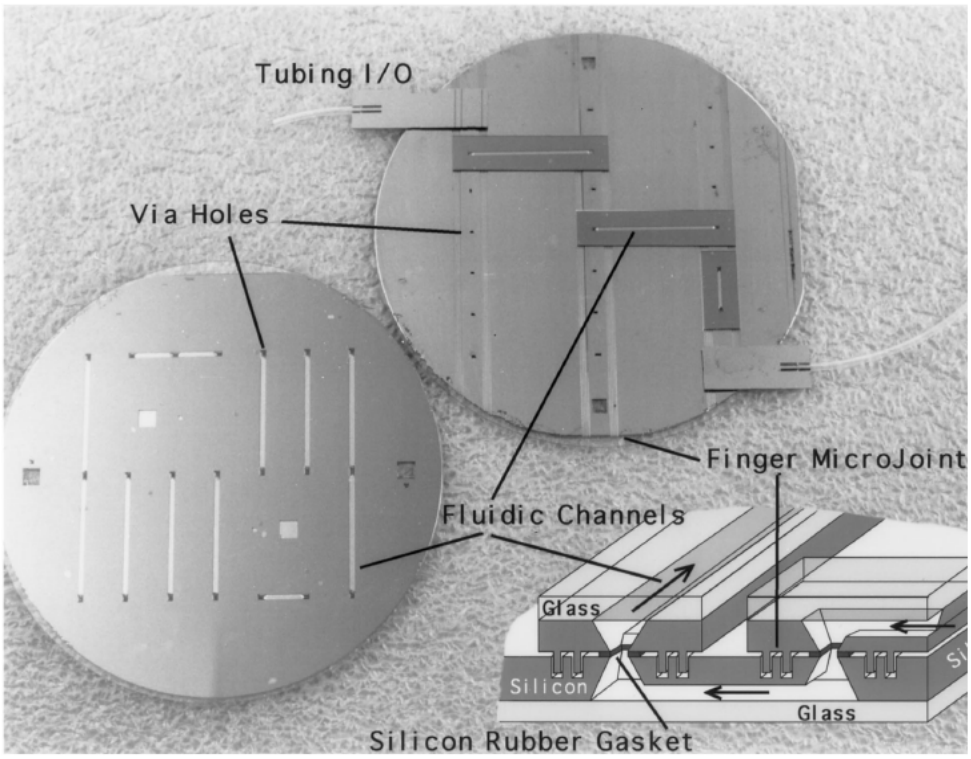

Figure 19. Assembled microfluidic system [5]

Jr-HungTsai et al [6] presented research work directed towards a tubing interconnection system that utilizes a Mylar (DuPont Mylar 50M44) grommet type seal. They used two different

methods for developing the Mylar seal approach. The first Mylar seal is made by manually cutting the Mylar film into 3mmx3mm squares. The capillary tubes are used to penetrate the Mylar film with the PVDC coating from the film touching the tube. The tube is then inserted into the microfluidic devices desired inlet/outlet location. And finally, some adhesive (SUR-LOK instant glue) is applied around the substrate, film, tubing joint (Figure 20). The other method requires fitting a piece of Mylar film to match the face of the substrate. The Mylar film is bonded to the substrate, there is a photoresist applied and patterned, the Mylar film is etched into a similar configuration as before. Again the capillary tubes are poked through the film squares and the adhesive was applied (Figure 21). This method requires multiple steps, complex processes, manual assembly, and is not repeatable, precise, or reliable. There exists a possibility for leaks around the Mylar to capillary interface and the Mylar to substrate interface. The glue has a propensity towards bubbling, which can be a source of a leak or structural failure. The inlet/outlet, microchannel, and structural support should be one piece. The research presented in this thesis is directed towards this one-piece construction.

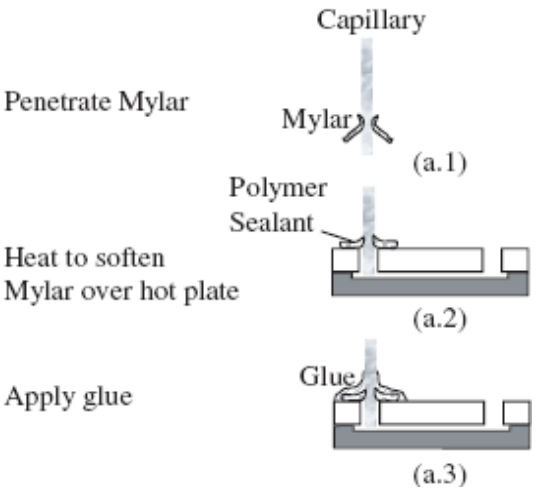

Figure 20. Schematic drawing of First method [7]

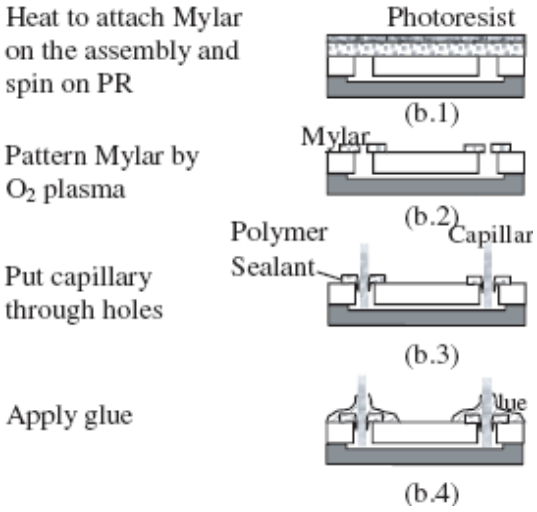

Figure 21. Schematic drawing of Second method [7]

B. L. Gray et al [7] explored and improved some previous research from C. Gonzalez et al [5]. In 2004, B. L. Gray presented two parts of a microfluidic interconnection system. The first part consists of an interlocking fin arrangement (Figure 22). Two pieces have matching fins and spaces that interlock. Each piece has its own microfluidic channels and one piece has a rubber or wax gasket to mate the opposing microfluidic channels. Instead of being fabricated by a saw, this time the pieces are fabricated using DRIE. The second part is comprised of mating pairs of holes and notched cylinders (Figure 23). The seal for the holes and cylinders are made of a wax gasket. Although very accurate, DRIE is not a feasible or practical fabrication technique. The DRIE process requires a high power plasma source. Even a short run of 100 pieces would be very timely and costly.

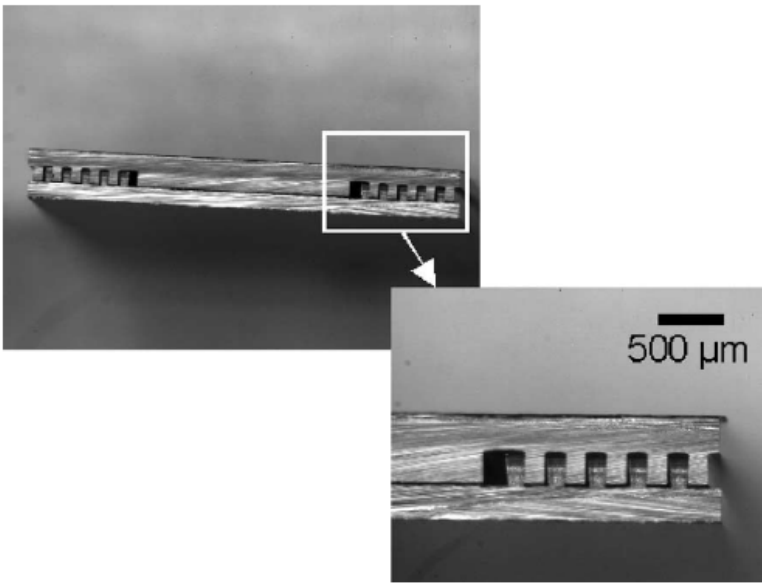

Figure 22. Interlocking fins by DRIE [7]

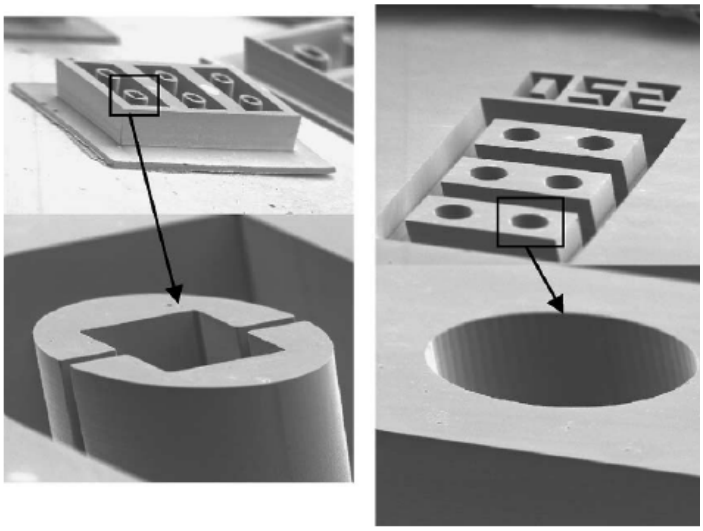

Figure 23. Hole and cylinder arrangement [7]

Eunice S. Lee et al [8] presented research work in 2004 which involved removable tubing interconnects and threaded interconnections machined into a glass substrate using Electro-

Chemical Discharge Machining ECDM. In ECDM, a cathode, an anode, and the substrate are submersed in a NaOH solution (Figure 24, 25).

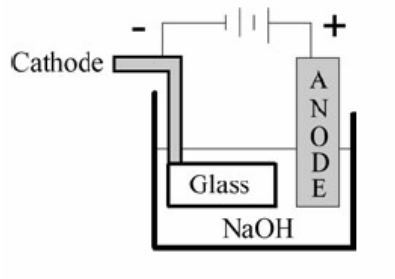

Figure 24. Schematic of ECDM process

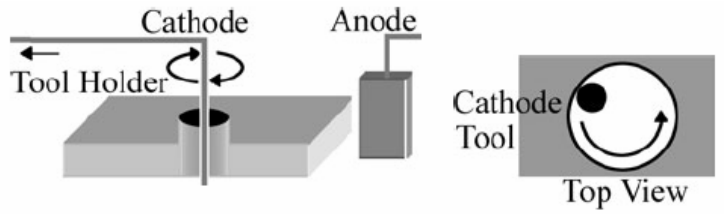

Figure 25. Schematic of using ECDM for different shape

By moving the cathode in relation to the substrate, the substrate can be machined into various shapes. For the removable tubing interconnect, a cone shaped hole was created on one side of the substrate and an identical hole was created in the opposite side of the substrate. By combining these two cones, a hole with a cross section shaped like an hourglass (Figure 26) can be created. Due to the shrinking inner diameter of the hourglass shape, a flexible tube is compressed when pushed into the hole. This pressure creates a seal (Figure 27). The seal is quite limited in the amount of pressure it can withstand. The threaded interconnection begins with the same ECDM process, only the ECDM is continued until the cross section becomes a straight hole (Figure 28) with constant inner diameter. An ECDM cathode with the proper thread pattern must then be

used in place of the old cathode to create the threading on the inside of the hole (Figure 28). Once the threaded hole has been made, a melted polymer is poured into the threaded hole. Using the threaded hole as a mold, a threaded fitting is created in the molten polymer once it solidifies (Figure 28). This interconnection requires a serial process of EDCM and the quality of threading is questionable.

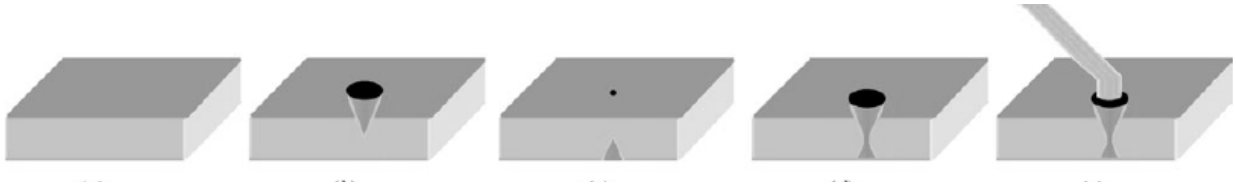

Figure 26. ECDM progression for hourglass hole [8]

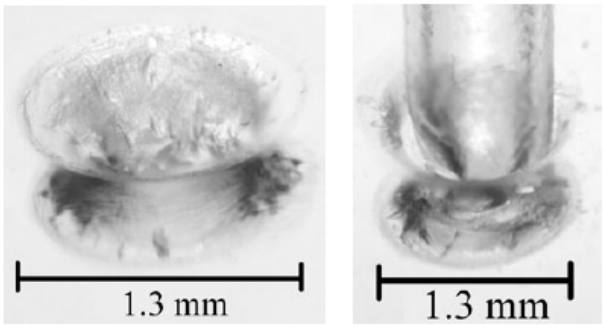

Figure 27. Pictures of hourglass hole and picture of hole with tube [8]

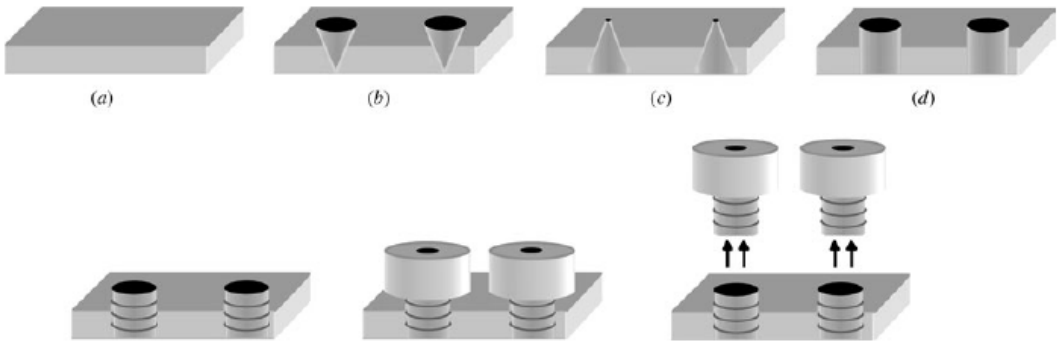

Figure 28. Schematics steps of creating the threaded interconnects and molding the threaded plugs [8]

Microfluidic handling components are in great demand in the development of biological/biochemical sensors and devices. A more efficient and effective method for packaging, handling liquid samples, and communicating with the macro world would have a tremendous impact on these devices. In contrast to electronic packaging, microfluidic packaging is more challenging due to a lack of standardized platform. In most cases, the liquid samples are introduced to the microfluidic device through input/output interconnections that are usually assembled manually. Holes are created on a solid substrate by various methods such as drilling [9, 10], reactive ion etching [11, 12] and electrochemical discharging [13], which are later used for the attachment of tubes. The interconnection process is often completed by applying an adhesive or thermal bond between inlet/outlet tubing and the substrate. Other approaches require the introduction of an intermediate coupler made of a silicone rubber ring [14]or a heat shrink polyolefin sleeve [15]. For layer-by-layer connections, interlocking silicon fins and hole-cylinder pairs formed by DRIE [16, 17], electroplated gold bumps [18] or peg-hole pair fabricated by stereolithography [19] have been used. Most of these require a separate step of hole preparation, tube attachment and alignment for the interconnection.

1.1.3. UV-LIGA

One fabrication technique that has shown much promise in accuracy, price, and expediency is UV-LIGA. It is capable of aspect ratios up to ~40. UV-LIGA is an adaptation of what is originally referred to as LIGA (a German acronym for Lithografie, Galvanoformung, Abformung meaning lithography, electroplating, and molding). LIGA is a micromachining technique that originated in the 1980s at the "Karlsruhe Nuclear Research Center. The original process utilizes highly parallel x-ray synchrotron radiation as a light source and a mask that also requires some extensive micromachining processes to be developed. UV-LIGA, on the other hand, uses ultraviolet light, a much more simple mask, and much less time.

As early as 1997, Zheng Cui et al [20] was presenting research on employing a photoresist as a sacrificial layer during a UV-LIGA process. The photoresist is spun onto the substrate, patterned, exposed, and developed (Figure 29). Now a second layer is put down in the position necessary to support future free-standing structure. A thin metal seed layer is electroplated on the second layer and another photoresist sacrificial layer is spun and patterned onto the seed layer. Finally the structural metal layer is electroplated over all of this, the seed metal is removed, and the sacrificial layer is dissolved (Figure 30). Although the metal mold fabricated by this method is robust, the entire process time is long and the mold needs other conventional machining steps to be used for a replication process. My research presented in this thesis will reveal the use of SU-8 directly as a mold tool for injection molding.

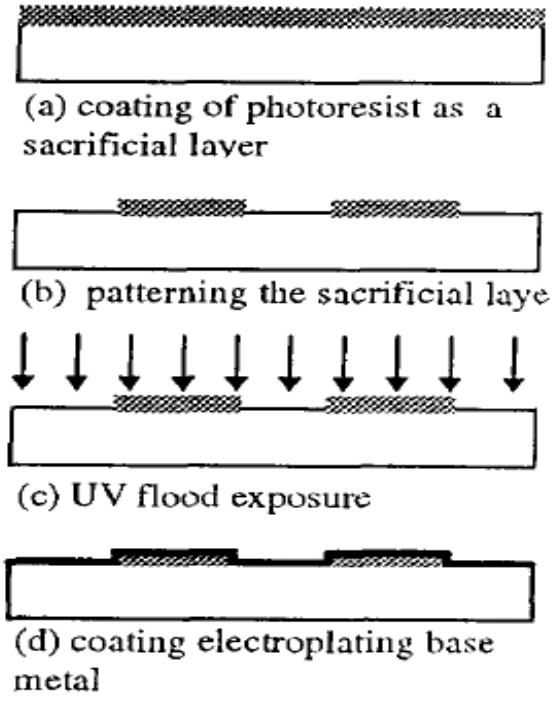

Figure 29. Initial UV of a sacrificial layer plus the seed metal layer [20]

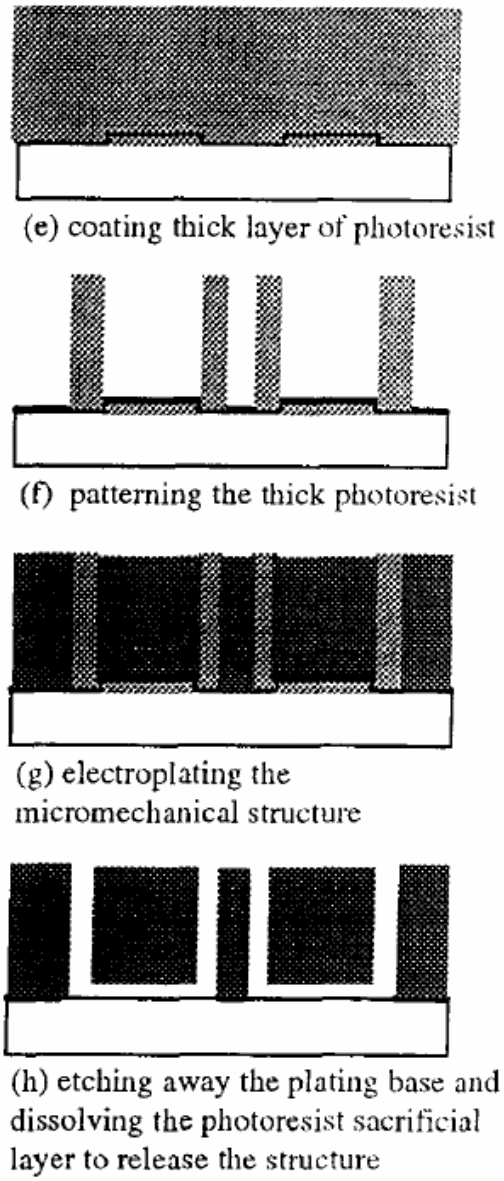

Figure 30. Schematic of second sacrificial layer and second seed metal layer [20]

Research presented from Fan-Gang Tseng et al [21] proposed a UV-LIGA process utilizing a different kind of photoresist. To avoid one of the problems associated with the use of SU-8 in a UV-LIGA process, that of SU-8 being difficult to remove, the author uses JSR THB-

430N. By using a lower spin rate with this photoresist, a thickness of 1.4mm was achieved. After soft baking at 100˚C for 7hrs, the photoresist was exposed to UV light of 365nm at 22,400mJ/cm^2 under a contact aligner, and finally developed inTHB-D1 developer for 1 hr with 40 kHz 26W ultrasonic agitation. Once the high aspect ratio parts (Figure 31, 32, 33) were developed fully, the parts were plated and then the photoresist was stripped away in acetone. This process works well for a single part, then the entire process would need to be repeated to generate another piece. In this thesis, the focus is small-scale batch fabrication, rapid reproduction, and standardization. If a material suitable structurally for a particular job were used as a photoresist, the plating and stripping processes would be unnecessary.

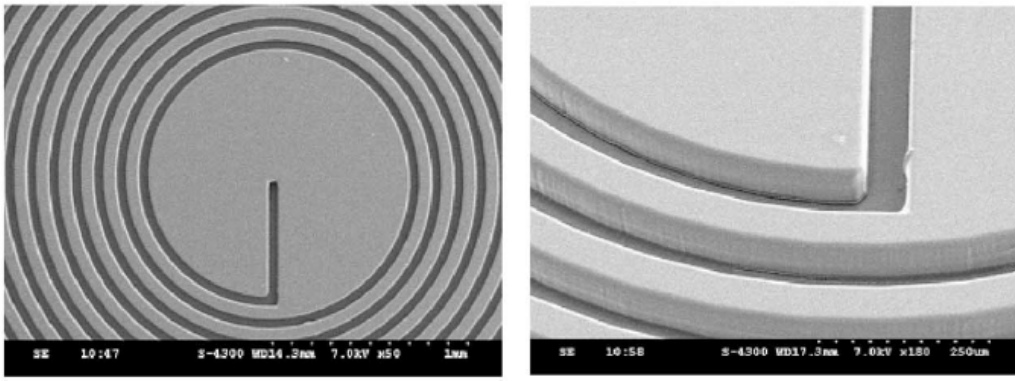

Figure 31. SEM pictures of high aspect ratio, high precision microparts: 66 mm coil mold and close-up

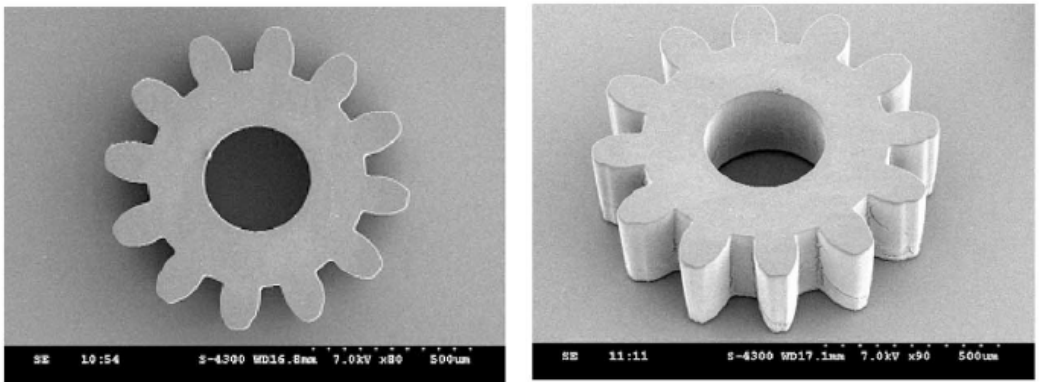

Figure 32. SEM pictures of high aspect ratio, high precision microparts: 257 mm thick gear and angle picture of gear

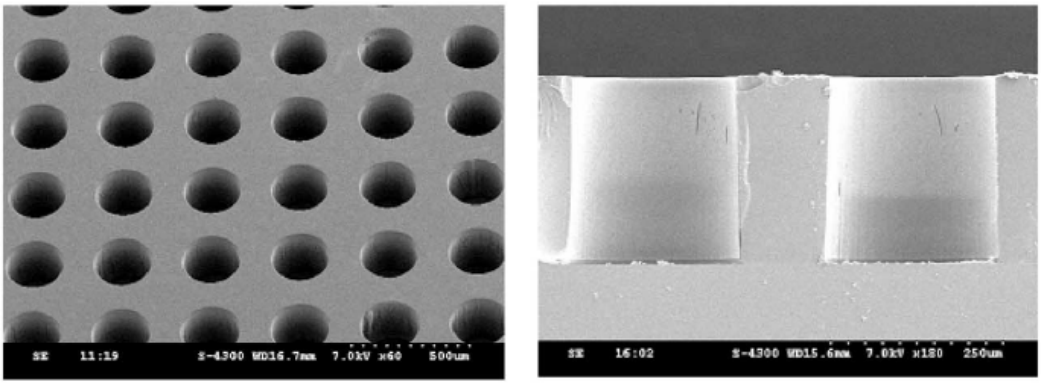

Figure 33. SEM pictures of high aspect ratio, high precision microparts: top view of close structure cross section of same

1.1.4. Anodized Aluminum

To generate a porous surface on an aluminum substrate, the process of anodizing was used. Anodizing is an electrical chemical process that results in the formation of a layer of oxide on the surface of aluminum that involves the utilization of a bath of dilute sulfuric acid as an electrolyte and the charging of the aluminum piece electrically. In the anodizing bath, usually a large lead plate is used as the negative pole or cathode. The electric charge and acid oxidation

create a thin film of aluminum oxide that is harder, less electrically conductive, and less susceptible to corrosion than the bare aluminum surface. At the same time, this oxide layer is very porous and uniform. The combination of chemically inert, electrically isolative, hard, porous, and uniform nanostructure on the aluminum substrate is very desirable for the UV-LIGA process.

Ahmed Nadeem et al [22] presented research work that encompasses the processes of masking, anodizing, and etching respectively an aluminum substrate. The desired result in this project is that of fabricating high aspect ratio microstructure from aluminum. The process was first to deposit and pattern a mask out of SiO2 (Figure 34) and then anodize the open aluminum (Figure 35). Once the open areas were anodized, they would be stripped in 5% sulfuric acid for 55 minutes leaving a very high aspect ratio and high-resolution 3-D aluminum microstructure in place of the oxidized areas. Although this process can generate some nice 2-D aluminum microstuctures, the entire process needs to be repeated for each part. This is not good for rapid replication. My research presented in this paper uses the anodization of the entire aluminum surface as a more adhesive substrate for the SU-8 that is then used to rapidly replicate as many parts as the mold remains in shape.

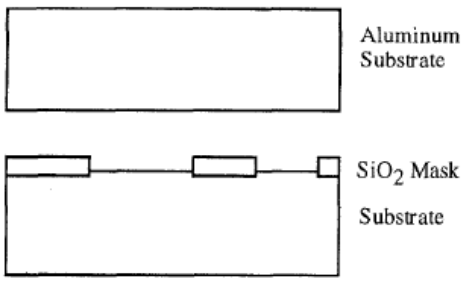

Figure 34. Schematic of masking[22]

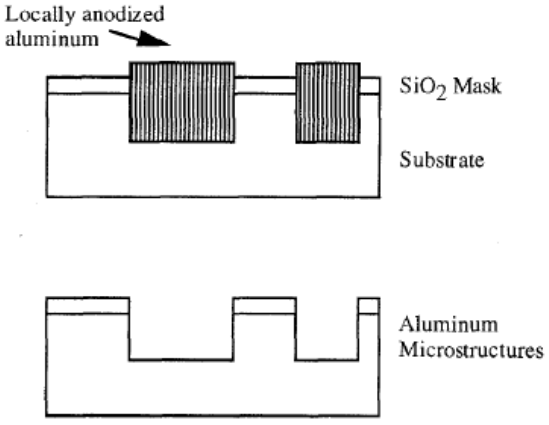

Figure 35. Schematic of anodizing and stripping[23}

S. Z. Chu et al [23] presented research in 2002 that investigated the various shapes and sizes of microstructures that were created by sputtering Aluminum onto a glass substrate. Highly pure, 99.99%, Aluminum was deposited on a soda-lime glass. The glass was previously coated with a tin indium oxide film and SiO_2 film. ITO (tin indium oxide) was a transparent and conductive medium to promote anodizing. SiO_2 film is used to prevent sodium in the glass from dispersing into the ITO film. The aluminum was sputtered on by rf-sputtering. Base chamber pressure was $1x10^{-5}$ torr, while the argon gas pressure was $2x10^{-3}$ torr. Sputtering power was 3.5 kW, and power density was$2x10^2$ kW/m^2. The anodizing was performed by a dc power supply (Nistac) at 130V in a 10% vol phosphoric acid. While anodizing the sputtered aluminum, one can see that the aluminum is completely consumed and transformed into aluminum oxide. This process produces a very ordered, symmetrical, parallel, oxide structure (Figure 36, 37). The research presented here uses an aluminum substrate.

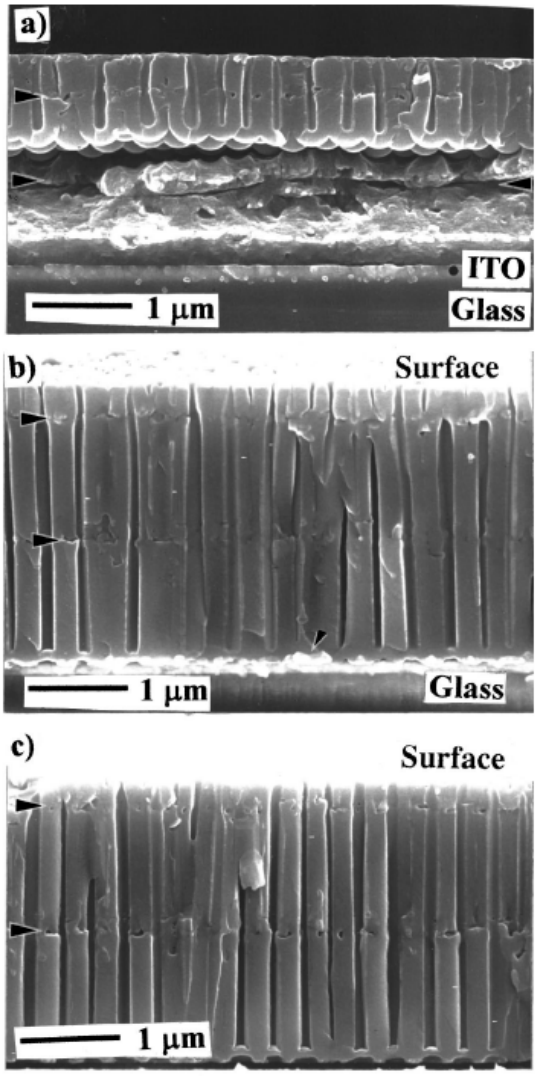

Figure 36. Field-emission scanning electron microscopy images a) 16min b) 46min c) 60min [23]

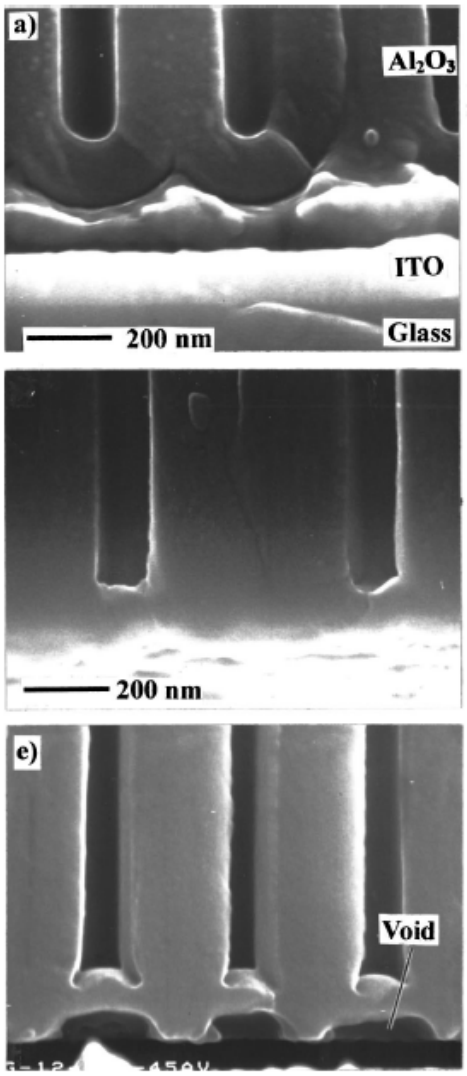

Figure 37. High-resolution FESEM a) 38min b) 45min c) 50min [23]

M. T. Wu et al [24] presented research that encompassed the various growth rates for aluminum oxide during an aluminum anodizing process. In this research work, the authors investigated the temperature and duration parameters of anodization on both a mechanically polished and an electropolished Al foil. The foil is a 1mm thick species of 99.97% purity from

Johnson Matthey of Ward Hill, Ma. The samples were degreased in acetone and mechanically polished using 1200, 1500, 2000, and 4000 grit polishing paper, respectively. After that, some of the samples were then electropolished. These parameters can be very helpful in the current research that is presented in this paper. Many of these conditions will be replicated for the purpose of generating a highly ordered nanostructure (Figure 38, 39, 40, 41).

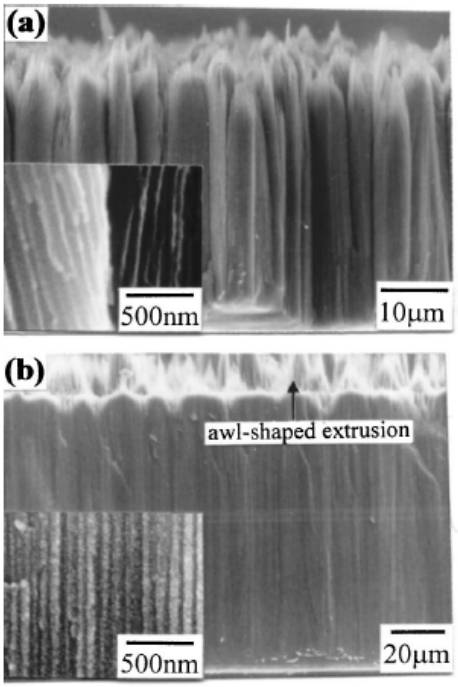

Figure 38. SEM Images of the cross sections of the oxides under conditions: a) 5˚C 72hrs mechanically polished b) 5˚C 72hrs elctropolished [24]

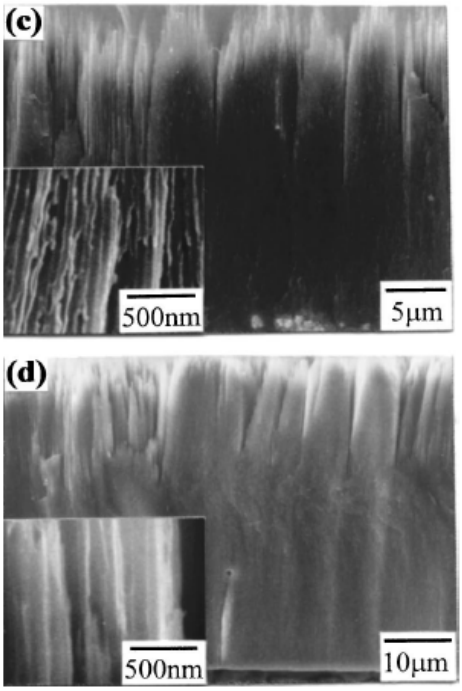

Figure 39. SEM Images of: c) 25˚C 72hrs mechanically polished d) 25˚C 72hrs electropolished [24]

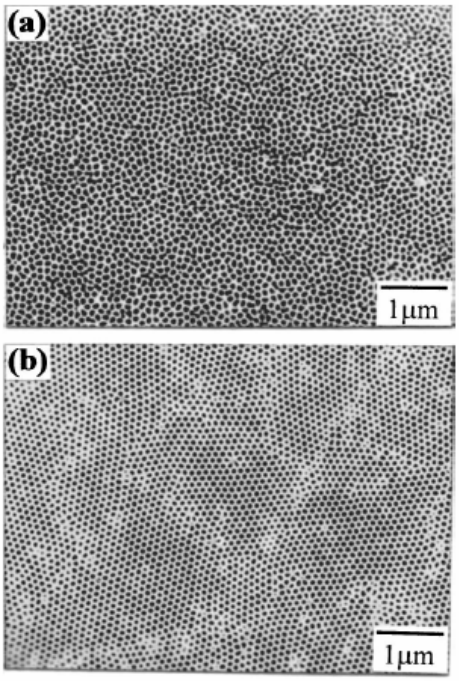

Figure 40. SEM Images of pore arrangements under conditions: a) mechanical polish all temperature b) 5C 72hrs electropolish [24]

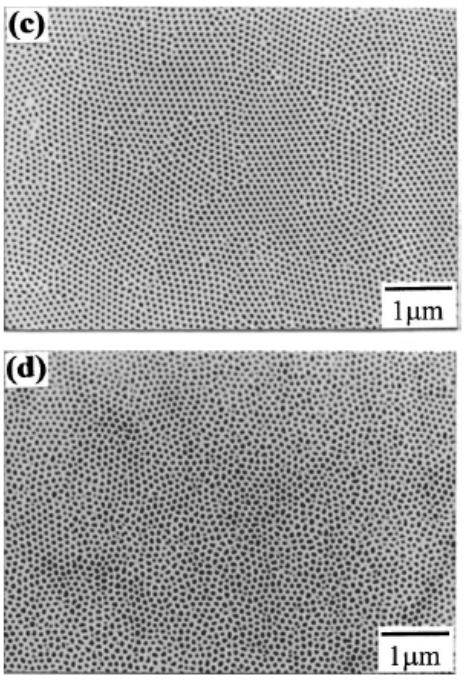

Figure 41. SEM Images of pore arrangements under conditions: c) 25C 12hrs electropolish d) 25C 60hrs electropolish [24]

R. Huang et al [25] presented research work in 2004 that was concerned with the relationship between surface roughness of an aluminum substrate and the resulting oxide film grown by anodizing the surface of that substrate. The research begins with an aluminum foil that is 100μm thick with 100μm typical grain size. These samples were immersed in NaOH solution for various lengths of time, they were washed thoroughly with DeIonized (DI) water, and finally they were dipped in HNO_3 at room temperature for about 1min., to avoid any erratic behavior from the NaOH. Anodization was carried out in a borate buffer solution with a current density of 2.5 mA/cm^2. For better imaging, the aluminum was dissolved in a solution of 10% bromine and

90% methanol, leaving only the oxide behind (Figure 42). This process led to the creation of cavities of average diameter of 66 nm with a standard deviation of 18 nm and a typical depth of 10-20 nm. Upon further investigation, it was realized that the number of voids scaled with the quantity of metallic interfacial voids present before anodizing.

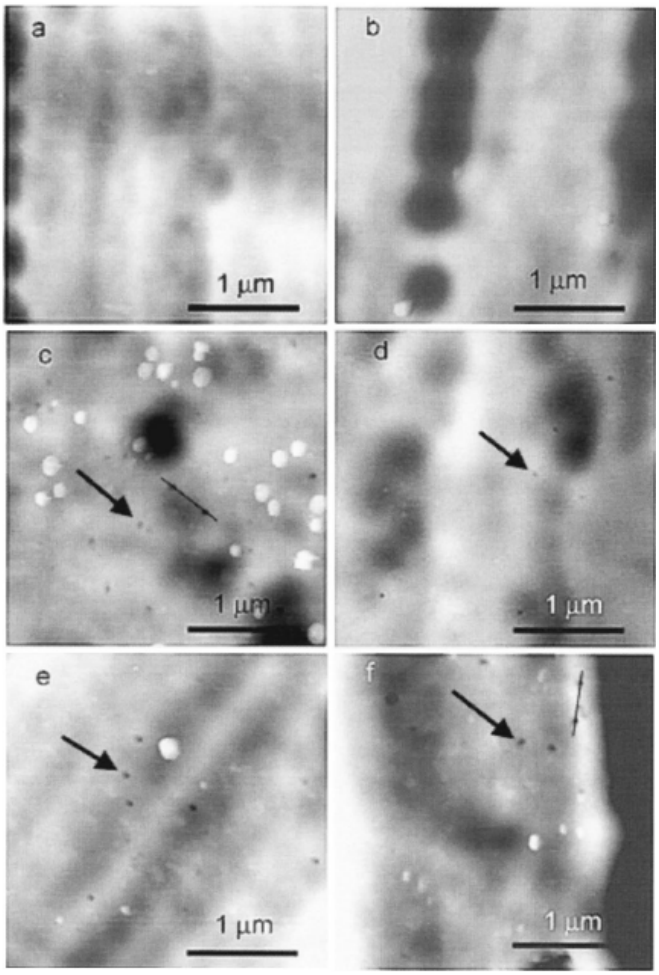

Figure 42. AFM Images after stripping of 106V anodic films. Stripping times:

a) 40s 17% removed b) 90s 38% removed c) 120s 50% removed d) 150s 63% removed e) 180s 75% removed f) 210s 88% removed

Xiaowei Zhao et al [26] presented their research regarding the anodizing behavior of aluminum masked with SiO_2 . Normally aluminum oxide grows in very uniform, parallel, ordered patterns (Figure 43). However when the aluminum substrate is masked by a SiO_2 pattern, a different sort of microstructure is developed (Figure 44). The process for this is as follows: first, the (99.999% pure) 0.3mm aluminum foil was pretreated by degreasing in acetone and ethanol, annealing (500˚C for 5hrs) was then performed on the aluminum to increase grain size. Then the aluminum was dipped into 2% HNO_3 for two hours and then the aluminum was electropolished. At this point, the SiO_2 was applied and patterned. The thickness of the SiO_2 was 400 nm. Anodization of the aluminum was carried out in 0.3M oxalic acid at 40 V and 1˚C. The longer that the etch process continues, the further under and more tilted the patterns of pores become.

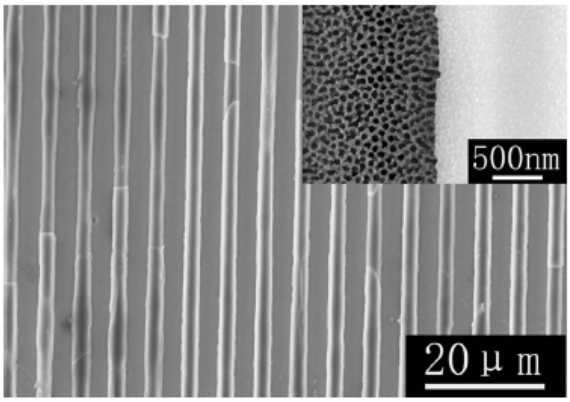

Figure 43. SEM Image of SiO_2 patterned aluminum oxide [26]

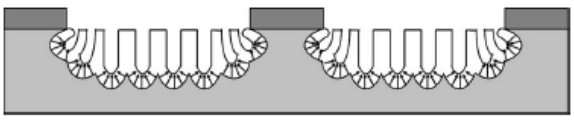

Figure 44. Schematic diagram of anodizing around SiO_2 mask [26]

1.2 Objective of study

The main objective of this study is that of developing more standard packaging style and rapid prototyping methods for it. This work is to accommodate our custom sensor design with packaging that interfaces with some industry standard for either the electrical communication or the fluidic communication or at times both. Rapid fabrication methods are studied by combining knowledge and methods from stereolithography, UV-LIGA, and nanofabrication. Ideally we would hope that given chip sensor and a general configuration for desired interface, these designs and/or packages could be useful in the development of a solution in the area of macro to micro communication.

CHAPTER TWO: DESIGN

The area of MEMS is a fairly new technology. Some of the standard procedures and processes are yet to be developed. This research work proposes some solutions to various BioMEMS type packaging necessary for biosensors. The three different packages presented here will be referred to as type I, type II, and type III.

2.1. Type I Package

A type I package was designed to accommodate a micromachined chip based sensor for flow through analysis. The fluidic package has an inlet and an outlet on one side to facilitate standard tubing connection while accommodating the fluidic channels and fluidic chamber on the other side. The schematic view of fluidic package structure is shown in Figure 45 and the side view, in Figure 46.

The inlet and outlet was designed for snap-in connections, which would not require any extra bonding step. Fluid analyte is introduced through the inlet/outlet tubing and flows through the microchannels into the sensor chamber which houses the sensor electrodes. In the chamber, sensors measure parameters from the fluidic sample. The analyte is then removed from the system through the fluidic channels that connect the chamber to the opposing inlet/outlet. The fluid analyte could now be introduced directly into another package and sensor system due to the serial connection capabilities of this package.

The Type I package was originally employed by Palsandram [27] for the measurement of KCl concentration in water.

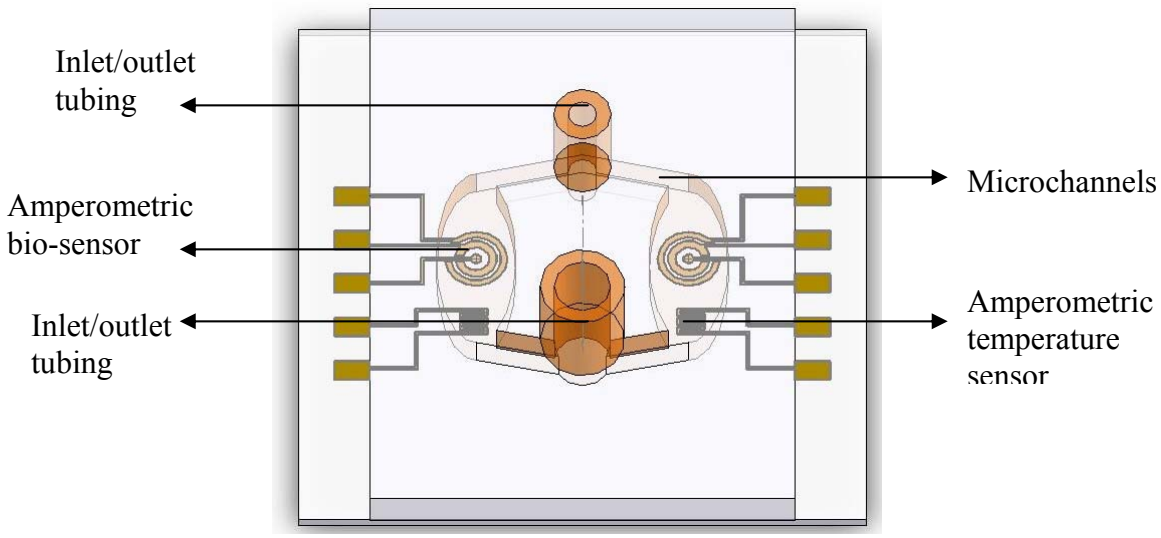

Figure 45. Isometric view 3D model from Solidworks - Package assembled with sensor chip

Figure 46. Side view 3D model from Solidworks Package only

In this design the inlet/outlet interconnecting tubes, holes, and channels could be made concurrently with a predefined mold. Therefore, an additional bonding or alignment step is not

required. The complicated assembly issue could be solved with type I construction by incorporating "standardized" tubing connections (e.g. 1/8", 1/16", 1/32" etc.). This standard design allows the system operator the opportunity to use many off-the-shelf fluid devices. Increases in the consistency, repeatability, and predictability of the measurements are inherent with this system.

The inlet/outlet interconnections were designed in such a way that the packages could be connected together in series. The internal diameter of the outlet is same as the outer diameter of the inlet. This design enables connecting multiple devices for a single sample flow using the standardized package platform.

2.2. Type II Package

The type II package was designed as a larger sample alternative to type I package. This package was designed to have an outer diameter of 3/8" so it could be inserted into commercially available snap-in tubing connectors. Thus, the housed sensor could work as plug-in type device in replacement of standard tubing in one of the ports. In this design, commercially available standard tubing and connectors for the tubing can be easily incorporated. The type II package does not require any bonding between the package and the electrochemical sensor. Instead in this configuration, the sensor is clamped between the two halves of the package. A preliminary adoption of this design concept appeared in Palsandram's work [27]

The package can be opened and closed repeatedly which allows for the sensor to be replaced. The type II package has a shallow cavity running through the center of it for the sensor to occupy. To maintain a connection between the sensor and the sample, the package is designed in

such a way as to locate the sensor portion of the sensor chip directly in the middle of the standard tubing, therefore the middle of the sample flow. The sensor body is then contained entirely in the package cavity. There is a very small lip that runs around the perimeter of the cavity that aligns and closes the package (Figure 47). The lip provides small amount of friction effectively holding the package closed while assembling or disassembling the pieces. The amount of friction necessary in the interlocking lip and groove for our purposes was an area of designing, fabricating, testing, and reiterating. The dimensions of the lip and groove were initially designed to fit very tightly together. This proved to be too tight and was very difficult to assemble. In each iteration of this design process the clearance was increased slightly (.01mm). The current configuration utilizes a .5mm wide lip and .55mm wide groove. These dimensions are close to the limits of precision of the machine, (.025mm).

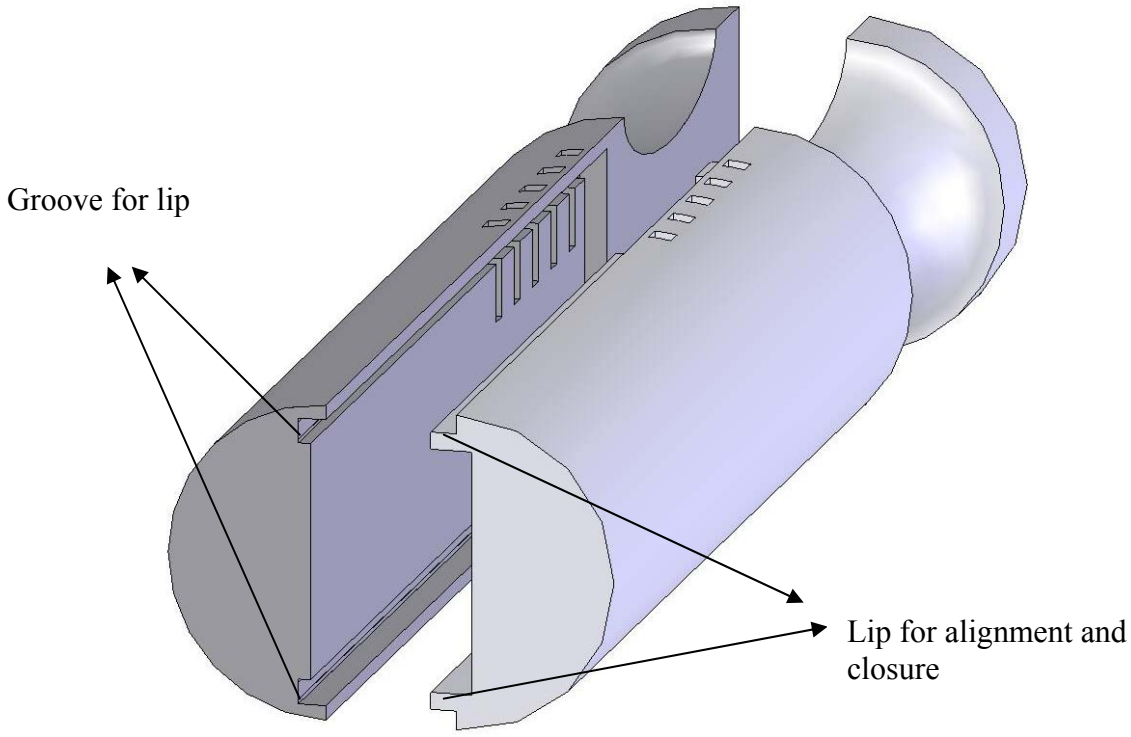

Figure 47. Picture from bottom view showing the lip of 3D CAD model

In Figure 48 one can see that the type II package has an area for locating the electrical leads onto the sensor's contact pads. The area created to accept the electrical leads is recessed slightly below the surface of the package cavity allowing just enough protrusion into the sensor as to make good electrical connection. The design of the areas for locating the electrical leads was also iterated in conjunction with the interlocking lip and groove iteration. The concern with this feature is that the electrical leads need to be positioned in such a manner as to make good contact with the sensor but not interfere with the proper closing of the package. The electrical leads were from a standard 5 pin commercially available electrical plug. The electrical leads have a square cross section that requires a square cross section for a hole. This hole shape is difficult to make by conventional machining, but easily made by stereolithography for prototyping or injection molding for larger scale production. The reason that this feature was designed as a covered hole rather than an open channel was for ease of assembly. It would be difficult to manually keep the electrical leads in alignment with the sensor while assembling the package. There are electrical leads locations on each half of the package for left or right side sensors. The 3D computer model was created in an engineering software package, Solidworks.

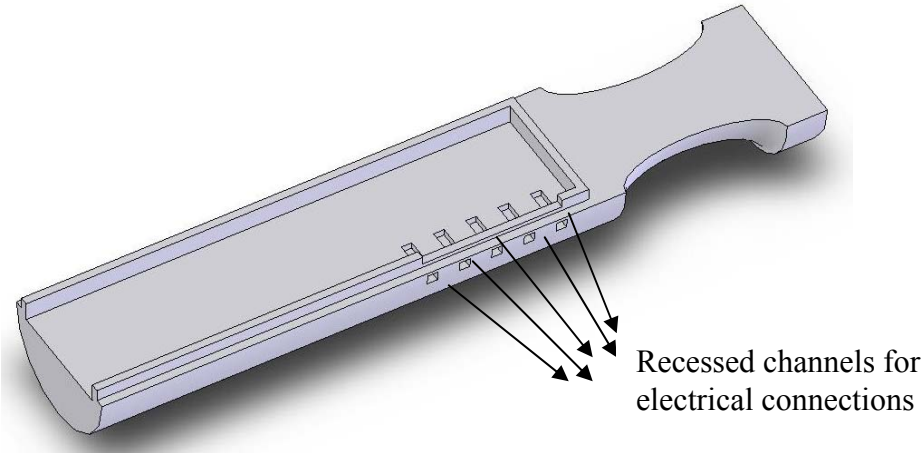

Figure 48. Top view of center cavity and electrical lead area

2.3. Type III Package

The type III package utilizes industry standards from the biomedical field, leur fittings, and capillary tubes. This design also inherently avoids the use of bonding techniques. The type III package accomplishes sealing and isolation of the sample and sensors by a compression o-ring. For this research rubber is fine. If an experiment calls for a different level of biocompatibility, the rubber o-rings can be easily replaced by a different material o-ring.

The type III package is set up for two sensors monitoring the same centrally located sample. The sample is extracted from the source through a glass capillary tube and deposited into a central cavity due to vacuum created by a syringe and due to capillary force in the tube. The syringe is attached to the package by a standard Leur fitting that is located opposite of central cavity from the capillary tube.

On two other opposing sides of the central cavity are locations for the biosensors. Locations for the sensors are basically recessed areas in the polycarbonate package. O-rings seals

are located in between the sensors and the central cavity. For ease of assembly, the o-rings have a slight recess to keep them located. The package is aligned, assembled, and compressed by four bolts.

This design required access for various features to a central isolated biological fluidic sample from four sides of the package. By arranging these feature accesses on the four sides of a cube, this leaves two opposing faces of the cube free for handling or experimental observation of the package. The material for this package was chosen for its reactivity towards our sample (very low) and for the optical properties (clear) of the material.

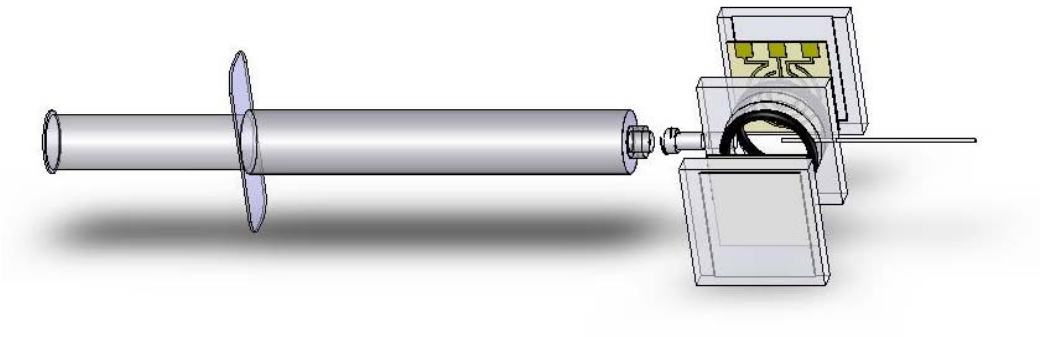

Figure 49. Syringe attached via luer fitting on Type III package

In comparison with previous research discussed in the background section above [5, 6, 8-12, 16, 17, 28-31], these package designs are an improvement due to their flexibility of use and their incorporation of existing standards for interface. The design of the Type I package incorporates the use of commercially available standard tubing sizes (1/8", 1/16") for easy connection to the inlet outlet features of the package. In addition to allowing the user to connect easily to off the shelf components, the one-piece design increases the strength of the package.

The Type II package is an improvement over previous research discussed above due to the ability to be reused for various sensors and interface with commercially available standard plumbing fixtures and commercially available standard electric plugs. The Type III package is designed to interface with biomedical standards for luer fittings, syringes, and needles. The Type III package is also reusable.

CHAPTER THREE: FABRICATION

3.1 Type I Package

Earlier in the design section of the thesis I mentioned that the type I package was created by injection-molding. The injection molding process that we employed is novel in that the microfluidic structure was fabricated from SU-8 patterned onto an anodized alumina structure. As a geometrically and structurally correct substrate, the existing mold fixtures from the manufacturer of the injection-molding were utilized. For attached tubings, one side of a molding block has cavities that could generate standard size inlet and outlet.

The microfluidic package was fabricated by injection molding using COC (cyclic olefin copolymer) resin. The COC polymer resin was melted to the liquid state at an elevated temperature and then injected into the mold. After the injection process, the mold was cooled down. The solidified part was ejected from the mold. The fabricated part is shown in Figure 50.

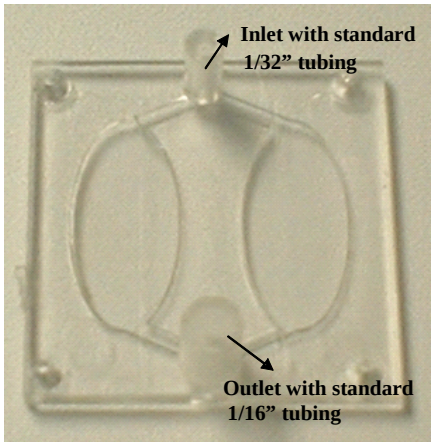

Figure 50. Fabricated Type I Package

The microfluidic package was fabricated by injection molding using COC (cyclic olefin copolymer) resin. The COC polymer resin was melted to the liquid state at an elevated

temperature and then injected into the mold. After the injection process, the mold was cooled down. The solidified part was ejected from the mold.

On the injection molding fixtures a layer of aluminum was deposited. Deposition was chosen on account of the resulting uniformity and purity of the deposited aluminum. The aluminum was then subjected to an anodizing process. Under the right conditions, the anodizing of uniform very high purity aluminum specimens generates a porous nanostructure. The nanopores are of importance to this process because they give the SU-8 a much better surface for stronger adherence. Now that there is a pore structure that the SU-8 can adhere to effectively, SU-8 is spun on. A mask for patterning was designed in the AutoCAD software to be transferred via photolithography. Normally in a UV-LIGA process, the SU-8 would now be electroplated. This step has been eliminated. The elimination of the electroplating is a tremendous savings in time and money. After developing the SU-8 on the mold fixture, the pattern is created on the exposed area as shown in Figure 51. The enlarged view of the protruded pattern is shown in Figure 52. The aluminum substrate that carries the SU-8 pattern was now inserted to a mold block and loaded into an injection molding machine (Figure 53). COC was heated to a liquid state and injected into the mold. The mold is cooled until the COC part solidifies and the final part is ejected from the mold. Figure 54 shows the replicated part and Figure 55 shows the detail.

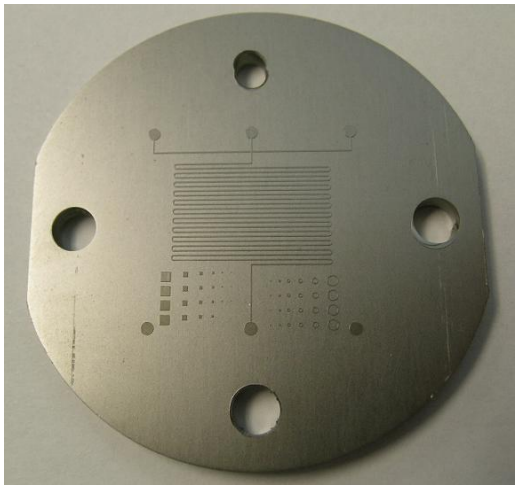

Figure 51. SU-8 micro structures on anodized Al substrate

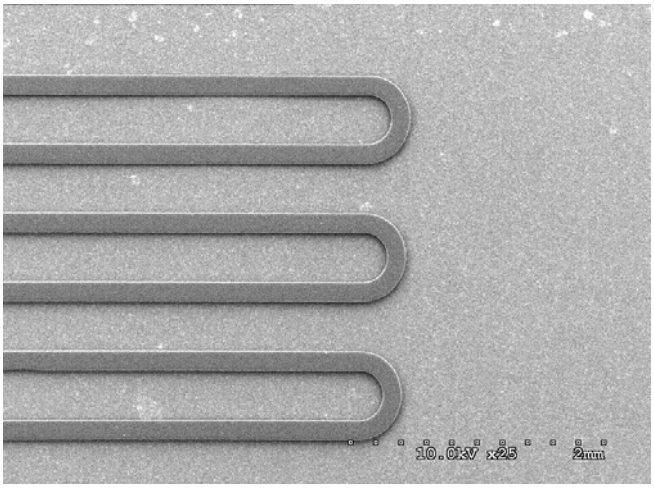

Figure 52.Details of SU-8 micro structure

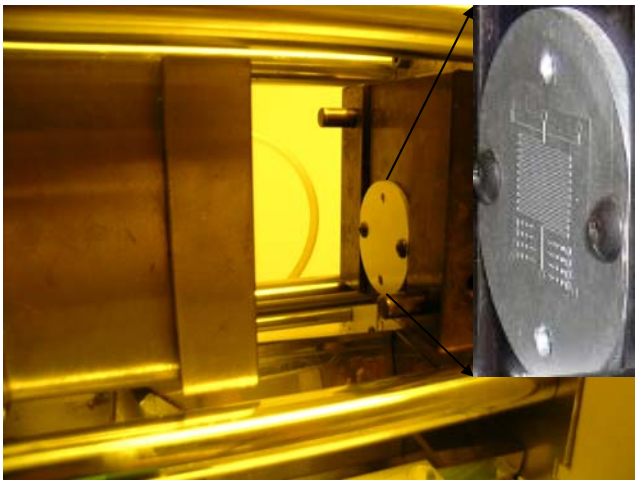

Figure 53. The mold mounted on the injection molding machine

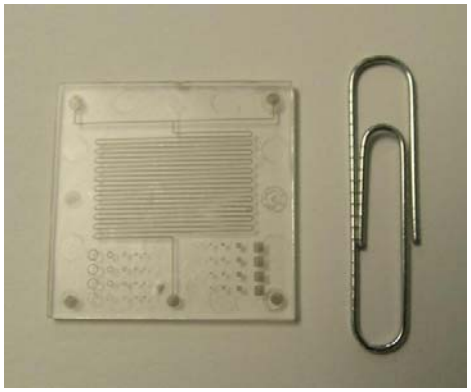

Figure 54. Replicated COC microchip

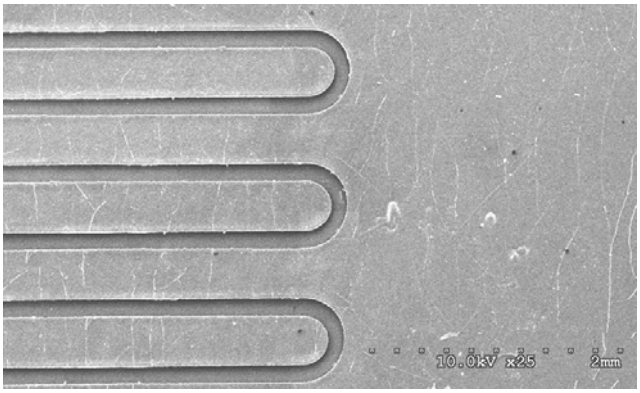

Figure 55. Details of the replicated COC microchip

As shown, rapid prototyping of microfluidic package and chip components was possible with a simplified process flow.

Figure 56 shows the packages interconnected with snap-in action due to one-body standardized tubing connection design.

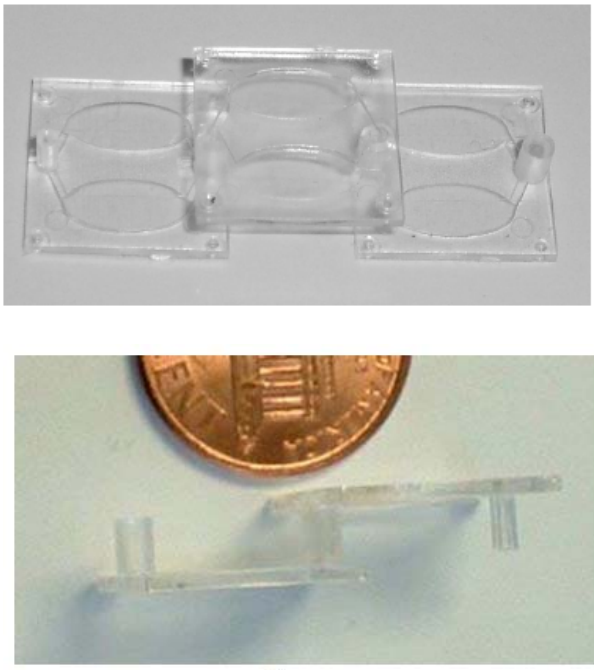

Figure 56. Pictures of Type I package interlocked at inlet and outlet

3.2 Type II Package

The fabrication of the type II package began with the computer modeling and design. Because the stereolithography process uses the direct 3D computer model to execute its processes, the computer model is an integral part of the fabrication process. This integration can cause some difficulties if one does not fully understand the relationship between the model and the stereolithography. Stereolithography will produce exactly what geometry is in the 3D computer model this includes what you cannot see or what you are not aware of. For example, a stereolithography machine could build a part that is composed of a thin hollow shell while a solid object was desired or vice versa. This is because the part appears the same whether solid or hollow. Many facets of this design really drove the fabrication in the direction of a

stereolithography process. Features such as the area for electrical lead connection and the interlocking lip and channel features made this package very difficult to fabricate with conventional machining. Because the stereolithography process fabricates 3D parts directly from a 3D computer model file that has been translated or "sliced" into thin 2D slices that are stacked successively on to each other, stereolithography offers the ability to create geometries that are not possible through conventional machining. One issue that has been discussed is the problem of fluid flowing into undesired areas of the sensor and package by capillary forces. Although this is a legitimate concern, this effect was never observed in our research. In the event of this occurrence, one could use a bio-inert gel or oil as a fluid barrier.

The Stereolithography Apparatus consists of a vat of liquid resin and an ultra violet laser arrangement (Figure 57). The 3D computer model described above is converted into several thin (as thin as the resolution of the machine can reproduce) 2D cross sectional slices. Each cross section slice is drawn individually onto the surface of the vat of liquid photosensitive resin. The resin is cured by exposure to the UV laser light and after each layer is cured, the support or stage is moved down a distance equivalent to the thickness of the layer that was just drawn. Once the stage has moved down the specified distance and a fresh layer of photosensitive liquid resin has covered the previous layer, the next successive cross sectional slice is drawn to cure this layer and this process repeats until the full model has been grown.

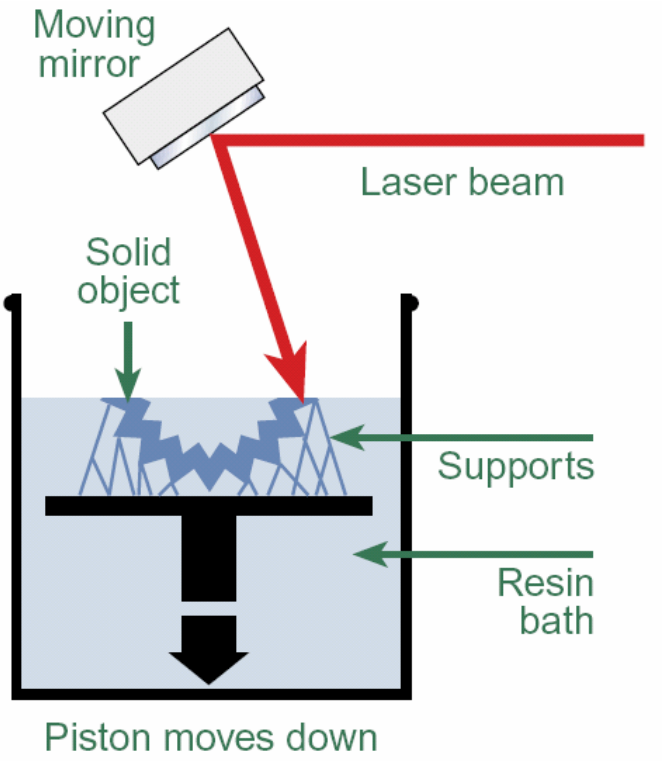

Figure 57. Schematic of stereolithography process

As one can imagine the resolution of the part is then limited by the number of and thickness of each slice. A large number of small slices create higher resolution and conversely a small number of large slices create lower resolution. Some features and geometries of the design may not be strong enough to support themselves until the complete structure has been cured. These are secured by a support structure, which is made by the same process at the same time as the desired part. The support structure is designed and built to be somewhat weaker and easier to remove than the actual part. When the build is complete the part is then drained, washed, and the support structure is broken away.

Figure 58 shows a fabricated type-II package before and after assembly. Figure 59 shows that the package can be fit into a standard T-connect allowing easy plug-in interface of a chip sensor with a flowing sample.

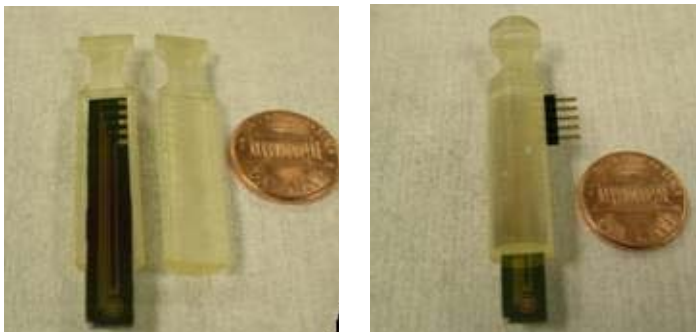

Figure 58. Type II package with sensor open and closed [27].

Figure 59. Type II package assembled with 3/8" standard fitting [27].

3.3 Type III Package

The type III Package was fabricated by precision machining (APPENDIX II, III). In this case, traditional machining techniques were used to create a recessed rectangular region for a chip type device, a cavity, a groove for O-ring seal, a hole for capillary tubing (or needle) and a tapped hole for luer fitting attachment (Figure 60). An assembled device with a chip sensor and a syringe is shown in Figure 60. Although this mechanical fabrication method is not cost-

effective, based on the same design a large quantity of type III packages can be fabricated using injection molding process. At this stage of investigation, the main focus was on proof of concept in type III.

Figure 60. O-rings are in black, the rectangles are the polycarbonate package components, bottom threaded leur fitting

Using an injection molding process would produce consistent, inexpensive, quality pieces. Whether fabricating the Type III package by machining or by injection molding, the final assembly would be by hand.

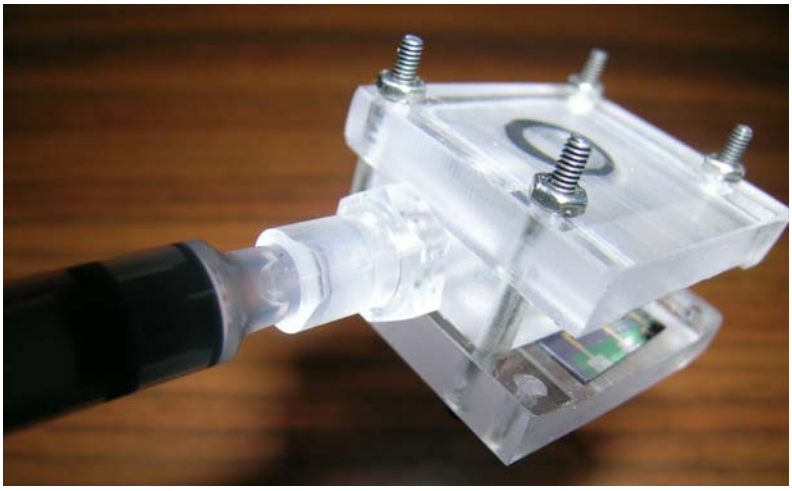

Figure 61. Picture of Type III assembled

As an improvement over research discussed above in the background section [2, 4, 20-26, 31-43], the novel fabrication technique in my research affords the researcher the opportunity to rapidly replicate small batch fabrication runs of prototype microfluidic designs with standard tubing interconnects already integrated. It is an adaptation of the UV-LIGA process that removes the electroplating and SU-8 stripping steps. This development cuts the time from design to injection molding fabrication from days to just a few hours. At the same time, the cost for production is greatly reduced.

CHAPTER FOUR: CHARACTERIZATION

4.1 Mechanical Testing

4.1.1. Type I Package

One concern in the implementation of the microfluidic package is that of structural integrity during service. For this, two tests were performed on type I. First, the test on the interconnection strength of the inlet/outlet tubing was conducted. A jig (APPENDIX II) was fabricated which held the pieces in the connected configuration with the axis of the inlet/outlet tubing aligned parallel to the axis of action of the M.T.S. Tytron 250 microforce testing system. Figure 62 shows a schematic of the test configuration. A jig was used to hold the interconnected microfluidic packages and a tensile force was recorded in the axial direction of the inlet/outlet tubing until separation occurred (Figure 63).

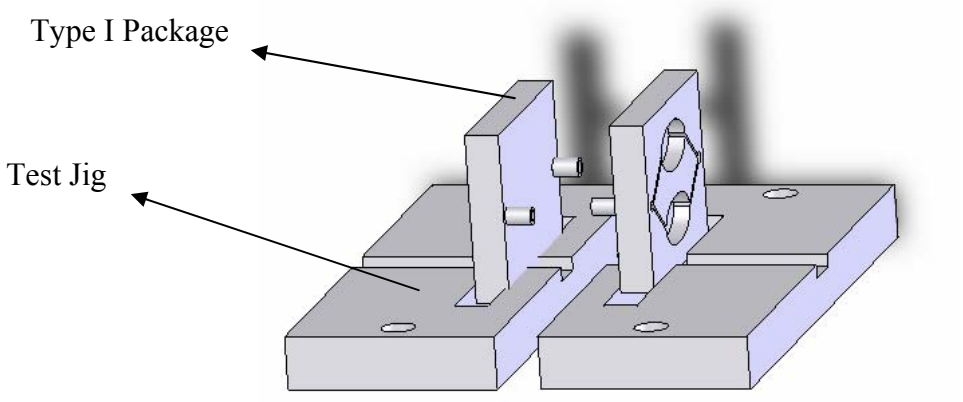

Figure 62. Conceptual model of package and jig

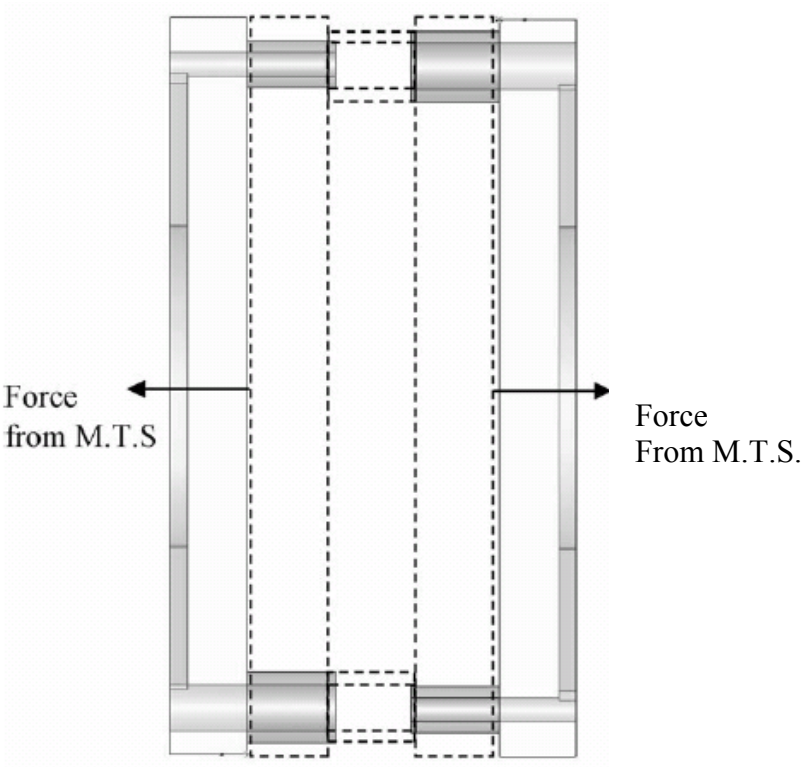

Figure 63. Top view for line of action in the separation test.

The resulting graph of force vs. displacement for disconnection is shown in Figure 64. A value of 1.38/2 N or 0.69 N for the separation force between one interconnected inlet/outlet tube was obtained. With the inner diameter of the tubing, the pressure required to separate the interconnection is calculated at around 1.373 MPa, which is higher than the common microfluidic application range.

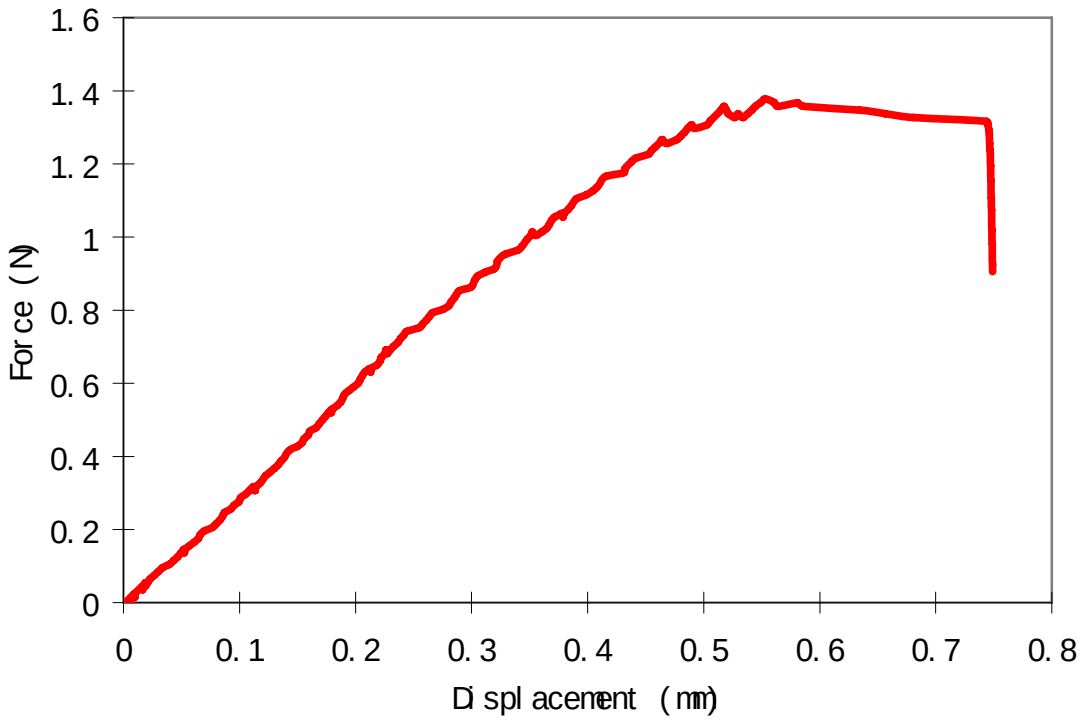

Figure 64. Force vs. displacement graph for interconnection separation

The second test was conducted to measure the bending strength of the inlet and outlet tubes. For this test, the package was placed in a jig (APPENDIX II) with the axes of the inlet/outlet tubes being perpendicular to the axis of force. The configuration of microfluidic package and applied forces can be seen in Figure 65.

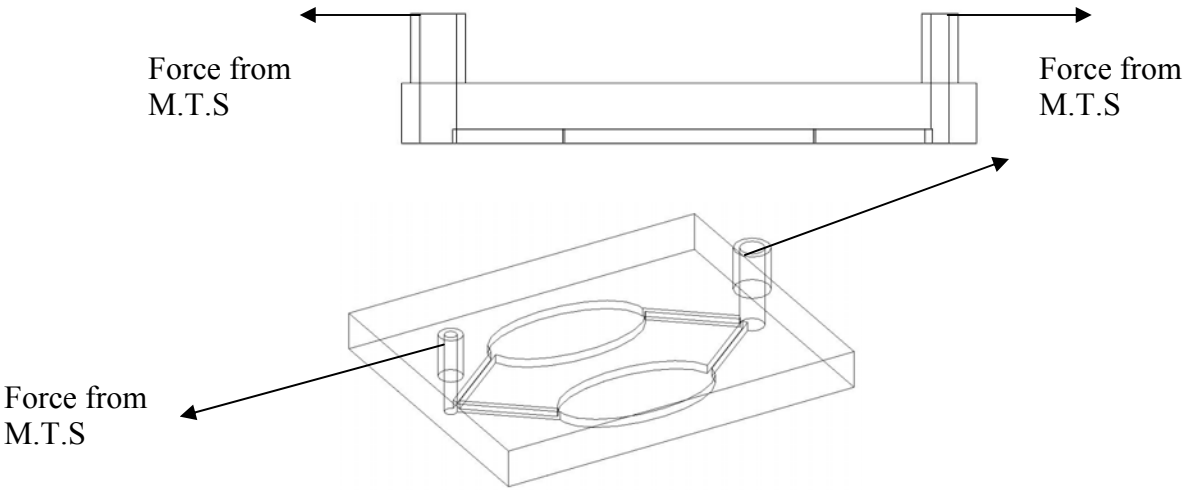

Figure 65. Schematic representation]n of inlet/outlet bending test

The jig was made such that the force would be applied close to the ends of the inlet outlet tubes while the body of the microfluidic package was constrained, generating a more accurate representation of response of the entire tube. The testing machine then applied force until one of the inlet/outlet tubes fractured. Figure 66 shows force and bending displacement in this test. It is observed that the yield occurs at 81.3 N in bending of the inlet/outlet tube. Compared to the reported value of 40.7 N in which a tube attached to a substrate was tested under tension [9], our integrated tube showed a much higher strength. It should be noted that the yield strength under bending is significantly lower than the yield under tension in general.

Developing a simple cantilevered hollow tube equation for this arrangement yields a similar result (Appendix I). For this mathematical model, the outer diameter of the tube was considered to be 1.6mm close to its base. This generated a load of 79N at a stress of 62.87 MPa (9118 psi).

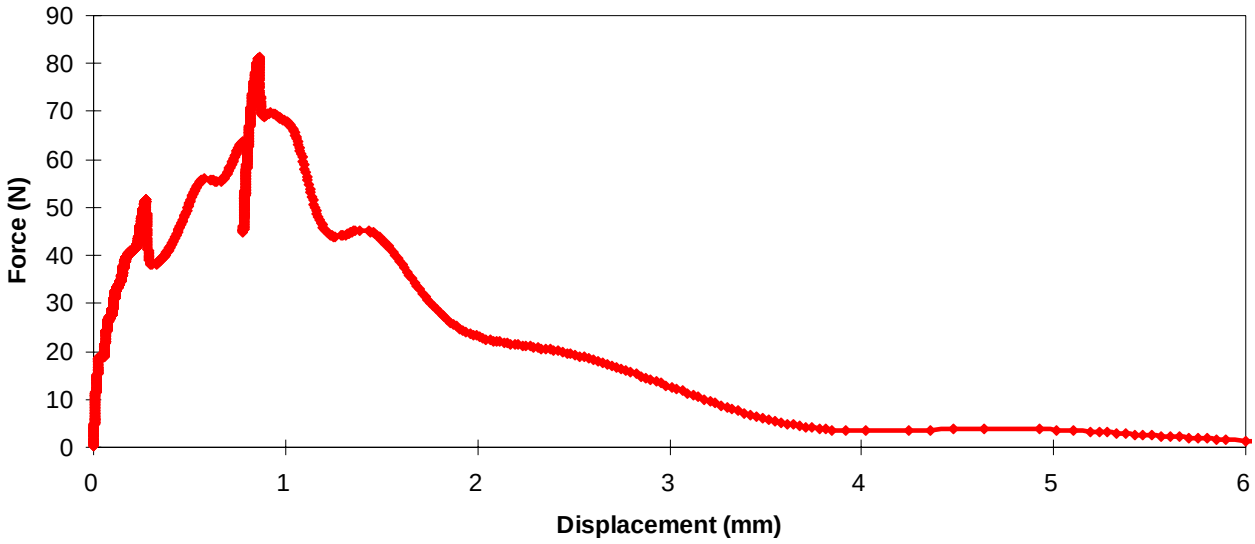

Figure 66. Force vs. displacement for type I package banding test on the inlet/outlet tubing

The test results compare very favorably to the computational simulation performed in a Finite Element Analysis software package called I-deas. As discussed above, the FEA models show a considerable difference in levels of stress concentration between our one-piece design and others' tube inserted into substrate design.

Two FEA models were created in the I-deas software package. A one-piece design representing our package was created according to the specifications and measurements taken from our physical piece and this model was assigned all necessary material properties according to the cyclic olefin copolymers properties. A multi-piece design representing the tube and adhesive in substrate state of the art was created which was comprised of three different models with three different sets of material properties that interacted through the FEA package's ability

to assign surface friction values between the pieces. The material properties used in these models were silicon for the substrate (yield strength of 26800psi), epoxy for the adhesive (yield strength of 15300psi), and nylon for the tubing (yield strength of 8000psi). Using identical loading (200N axial load at end of tube), boundary conditions, and critical geometries between a one-piece finite element model and a finite element model consisting of multiple pieces, the one piece model generated a peak stress of 9×10^4 Pa and a well distributed pattern of stress (Figure 67) whereas the model consisting of multiple pieces generated a peak stress of 1.43×10^6 Pa and the distribution was very concentrated around the interfaces between the tube and epoxy (Figures 68, 69).

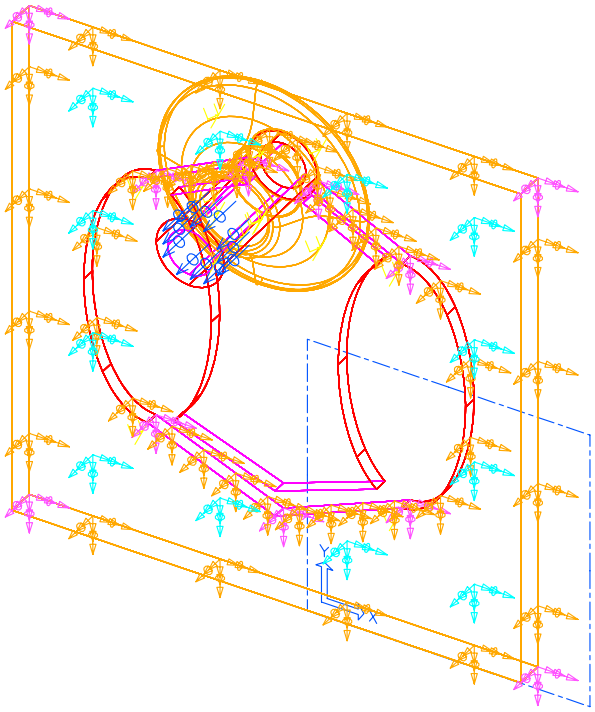

Figure 67. Boundary conditions on multiple-piece design. Blue = Force, Orange = constraint, Purple = constraint, Aqua = constraint

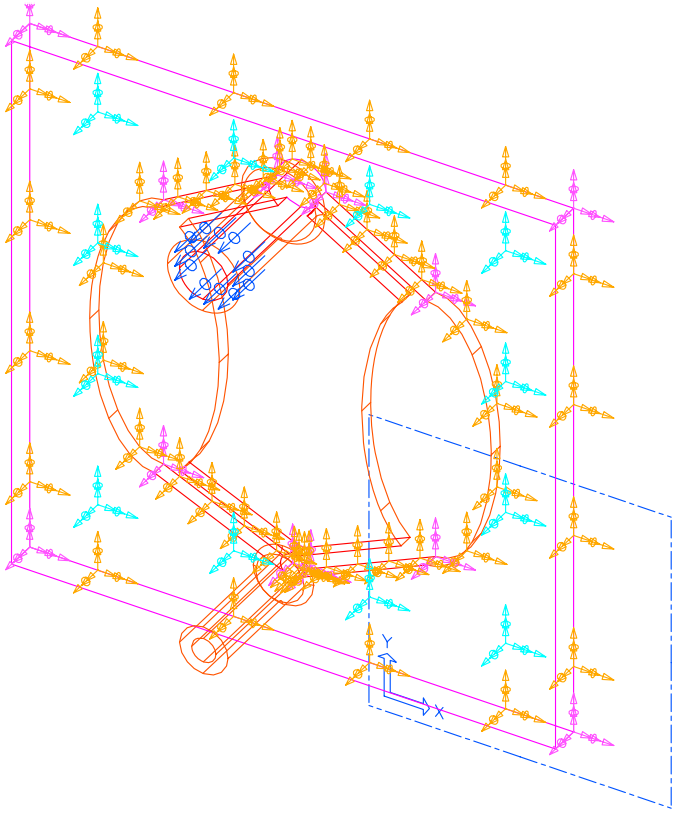

Figure 68. Boundary conditions on single-piece design. Blue = Force, Orange = constraint, Purple = constraint, Aqua = constraint

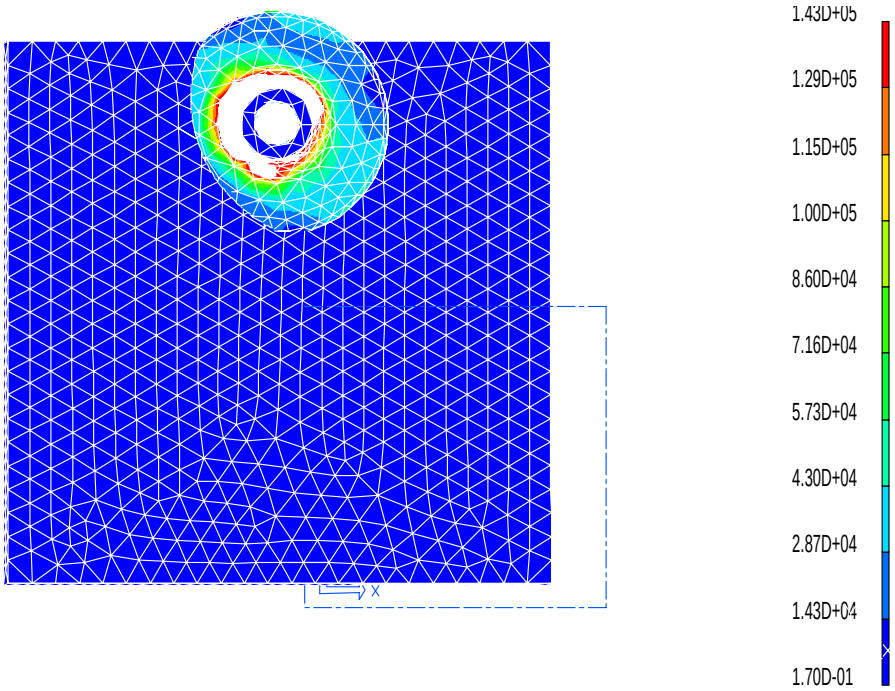

Figure 69. Finite Element Model of multiple-piece design (Front view)

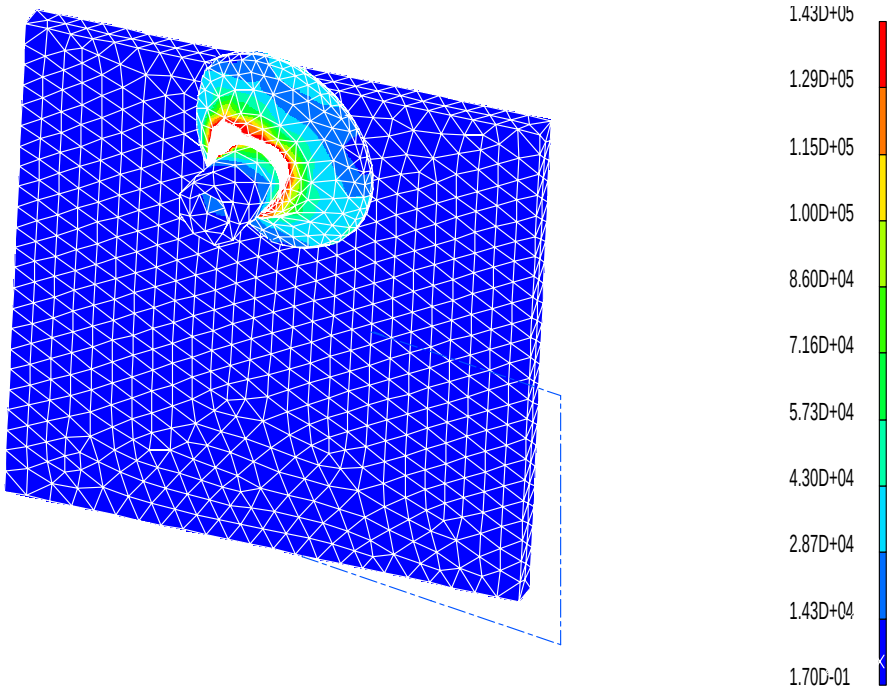

Figure 70. Finite Element Model of multiple-piece design (Isometric view)

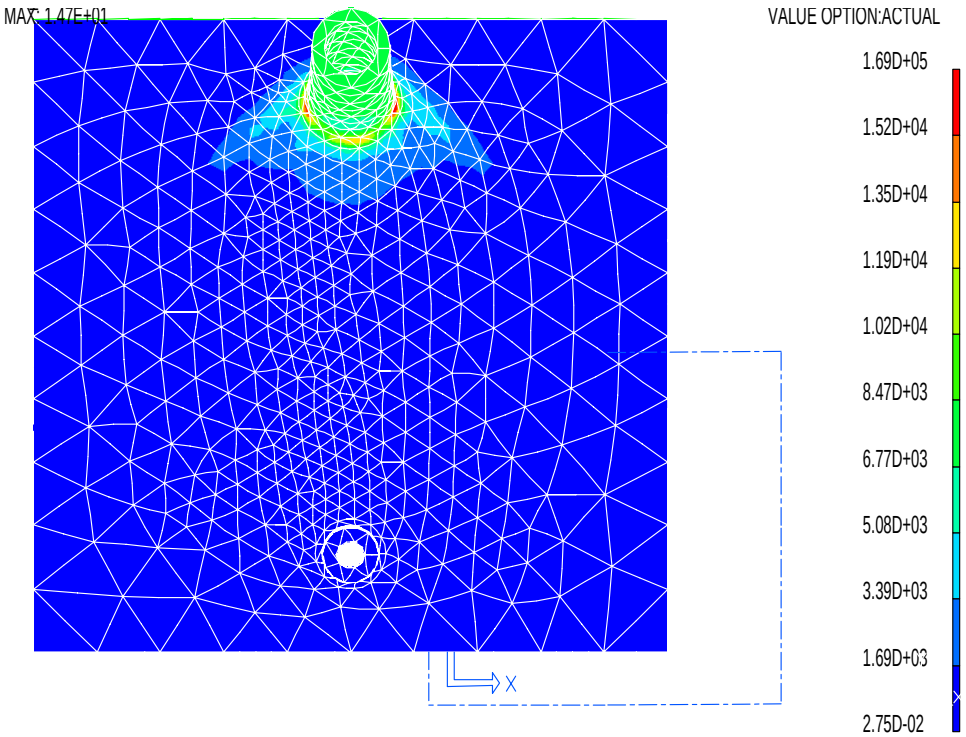

Figure 71. Finite Element Model of single-piece design (Front view)

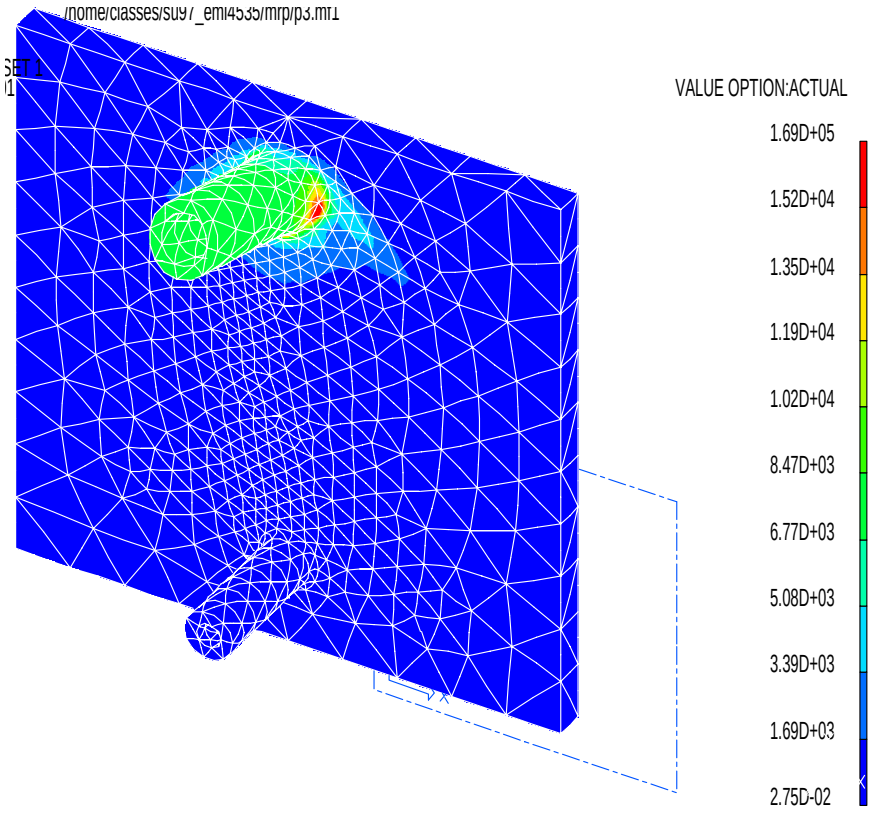

Figure 72. Finite Element Model of single-piece design (Isometric view)

4.1.2 Type II Package

The type II package was tested for tensile strength in an Instron Universal Materials Testing System machine. Again a jig (APPENDIX V) was fabricated for the purposes of applying the force in the desired location and configuration for the tensile test to closely represent the forces the package will experience in service. The type II package was loaded on the curved surfaces adjacent to the thinnest section of the "neck" (Figure 73). In service most loads will be on or adjacent to the neck of type II package and in addition, the neck being the thinnest section means failure is most likely going to occur here. The jigs had circular notches machined into them to apply a force around the entire neck rather than at a point.

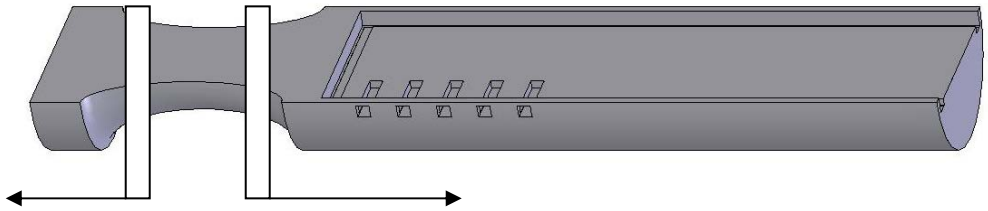

Figure 73. Schematic diagram of forces from Instron tensile test

Two separate halves of the package were tested under almost identical conditions. The package was loaded into the jig that fit loosely enough as to prevent the test from loading the package in bending or shear, only in pure tension. The Instron machine was set to apply a deflection of .5mm per minute, a total deflection of 5mm, or a total load of 1000N. Both tests resulted in similar deflections and loads. Test I resulted in a deflection at fracture of 3.46mm and a load at fracture of 411N (Figure 74). Test II resulted in a deflection at fracture 3mm and a load at fracture of 303N (Figure 75). It must be noted that neither packages fractured at the expected location likely due to imperfections and voids in the material.

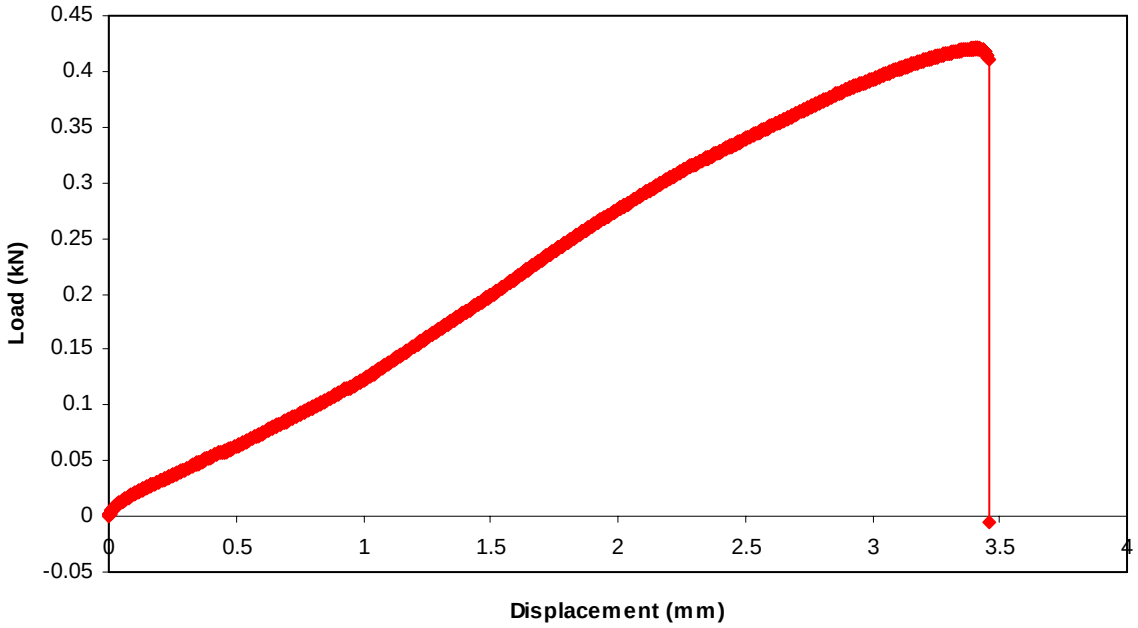

Figure 74. Graph of Instron tensile test for type II package.

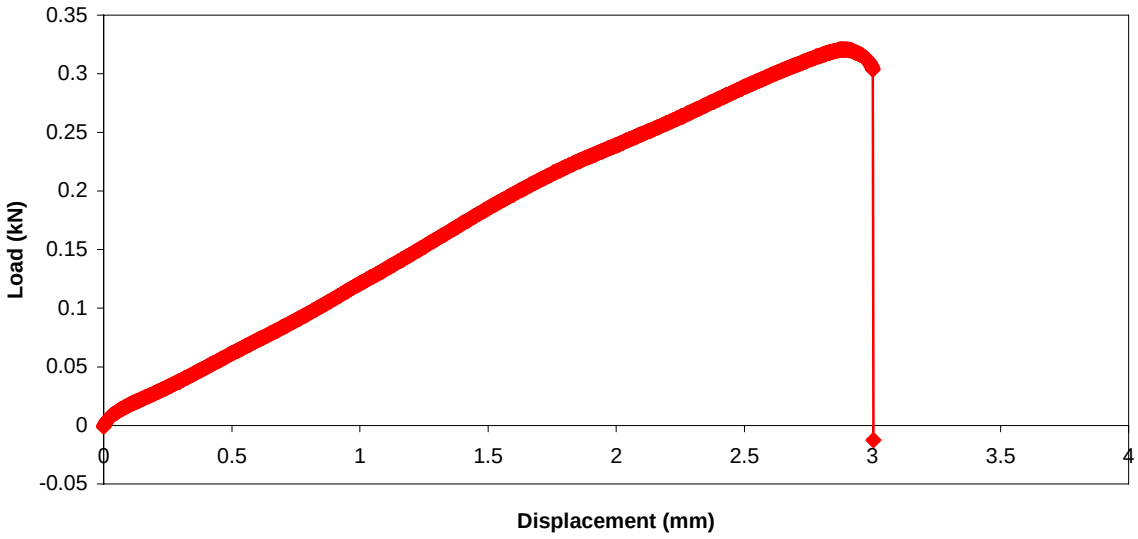

Figure 75. Graph of Instron tensile test for Type II package

A FEA simulation as developed for comparison of results. Using the material properties from the SLA material and the same 3D computer file that was utilized to create the stereolithograhy prototype, a load was applied of 400N in tension parallel to the longitudinal axis of the Type II package. The results are very good: The SLA material has a yield strength of 66-68 Mpa which is what the FEA model generated as a high stress in the thin neck portion of the model (Figure 76). The standard plumbing fixture utilized in service with the Type II package is rated for 250psi or 1.72Mpa, this value is much lower than mechanical limit of the package.

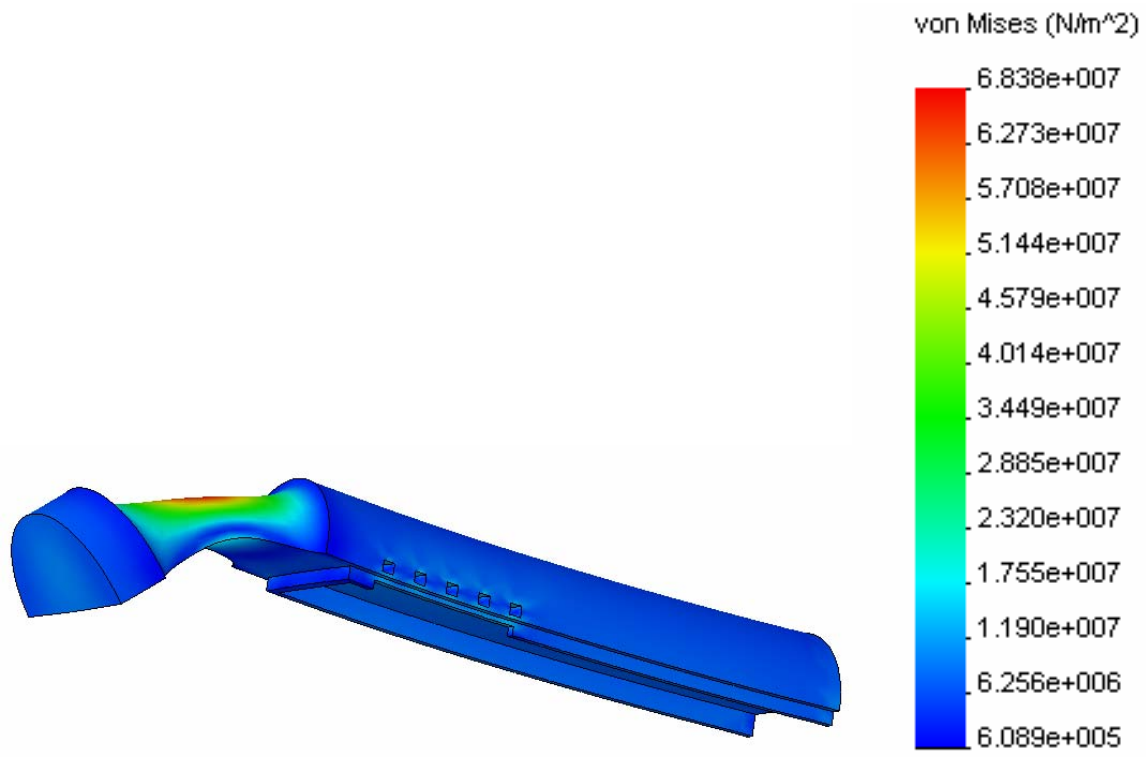

Figure 76. FEA of Type II package

The results from my testing, calculations, and simulations relate a strong improvement in the mechanical service strength of the Type I, Type II, and Type III packages over existing

designs presented earlier in the background section of this thesis [5, 6, 9-11, 13, 16, 28, 30, 33, 39, 44, 45]. I have shown significant Improvements in areas such as tensile strength, bending strength, and maximum fluid pressure. These improvements are related to a more simple design with fewer separate pieces.

CHAPTER FIVE: CONCLUSION

The research presented in this thesis involves the standardization of MEMS packaging and the design, fabrication, and characterization of said packaging. Using what exists commercially at the macro level to interface with what is being invented at the micro level is a necessary function in the integration of MEMS devices into the mainstream market. The production scale of current research into these products and areas has restricted the integration of new devices by cost and availability.

In this work, three different types of packages were designed, fabricated and tested. In rapid prototyping of these components, combination of novel and traditional micromachining techniques including UV-LIGA, stereolithography and precision machining were studied. In type-I package, a rapid production of microfluidic pattern using a SU-8 over anodized alumina structure was demonstrated with an injection molding method. Structural integrity of the fabricated package using a one body design was tested and compared with the previous results. The proposed method provides an alternative to produce a strong and inexpensive chip-type BioMEMS devices. In type-II package, the package was produced for large volume sampling with reiterated design and fabrication. As a result, a plug-in type package with standard electrical/fluidic connection capability was created. Its mechanical strength was studied with FEA model and standard tensile testing. The type-II package could be used to house a chip sensor in connection with standard size fluidic tubings and connectors. The type-III devices provide easy connectivity with a syringe for sampling, which would reduce a required time for testing a sensor.

Future developments will undoubtedly cause the evolution of microfluidics devices to parallel that of the microelectronics industry. All of this is dependant not only on the innovations of future work but also the economic forces caused by consumer demand.

The anodizing process has yet to develop the well-controlled nanoporous structure that we desire. This will be pursued further in future work.

APPENDIX I.

MATHEMATICAL CALCULATIONS FOR STRESS AND STRAIN IN PACKAGE TESTING VERIFICATION.

Calculation for cantilevered hollow beam of circular cross section

$L = \text{distance}_{load}$ $s = \text{distance}_{measured}$ $F = \text{load}$

$E = \text{Youngs}_{modulus}$ $I = \text{moment}_{inertia}$

$$\sigma = \frac{M_y \cdot c}{I} \qquad M = F \cdot d$$

$\text{coc}_{max\sigma} := 9100\text{psi}$ $\text{tube}_{od} := 1.6\text{mm}$ $\text{tube}_{od} = 0.063\,\text{in}$ $F := 79\text{N}$

$\text{tube}_{id} := .8\text{mm}$ $\text{tube}_{id} = 0.031\,\text{in}$ $d := .3\text{mm}$ $d = 0.012\,\text{in}$

$$\sigma := \frac{(F \cdot d) \cdot \frac{\text{tube}_{od}}{2}}{\left[\frac{\pi\left(\text{tube}_{od}^{4} - \text{tube}_{id}^{4}\right)}{64}\right]} \qquad \sigma = 9.118 \times 10^{3}\,\text{psi}$$

Calculation for internal pressure in microfluidic package to cause disconnect.

$\text{area}_{small.tube.inner} := \pi \cdot (.4\text{mm})^2$ $\text{disconnect}_{force} := .69\text{N}$

$$\text{pressure}_{max} := \frac{.69\text{N}}{\text{area}_{small.tube.inner}} \qquad \text{pressure}_{max} = 1.373 \times 10^{6}\,\text{Pa}$$

Calculation for tensile axial stress of hollow tube of circular cross section.

$\text{area}_{small.tube.material} := \pi\,(.8\text{mm})^2 - \pi \cdot (.4\text{mm})^2$ $\text{Stress} = \frac{\text{load}}{\text{area}}$

$\text{coc}_{max\sigma} \cdot \text{area}_{small.tube.material} = 94.613\,\text{N}$ $\text{coc}_{max\sigma} = 6.274 \times 10^{7}\,\text{Pa}$

APPENDIX II

MECHANICAL DRAWINGS FOR MACHINING OF TYPE I PACKAGE TEST JIG.

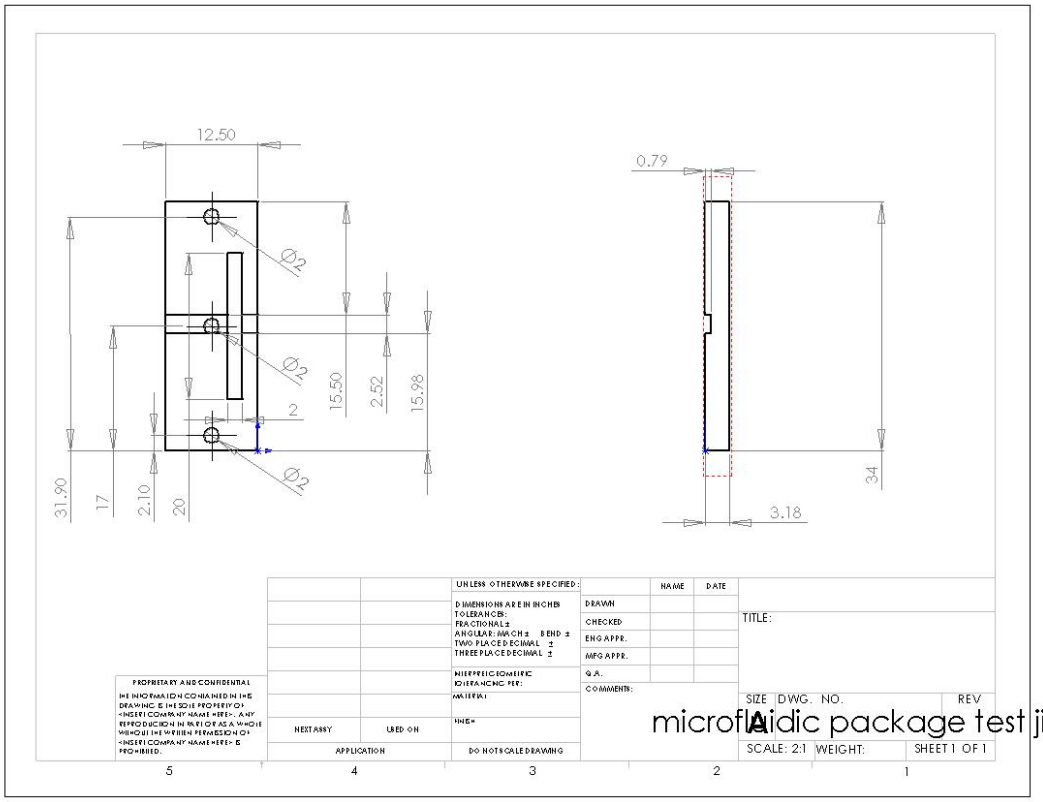

APPENDIX III

MECHANICAL DRAWINGS FOR MACHINING OF POLYCARBONATE TYPE III PACKAGE.

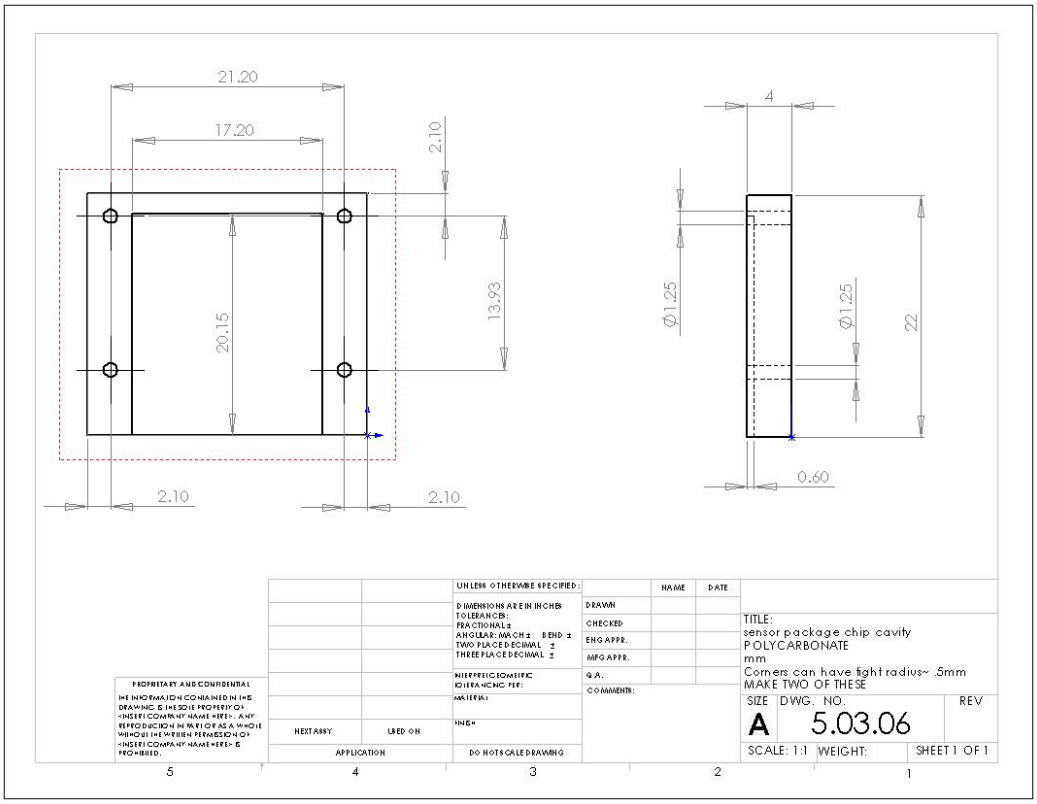

APPENDIX IV

MECHANICAL DRAWINGS OF TYPE III PACKAGE MACHINING.

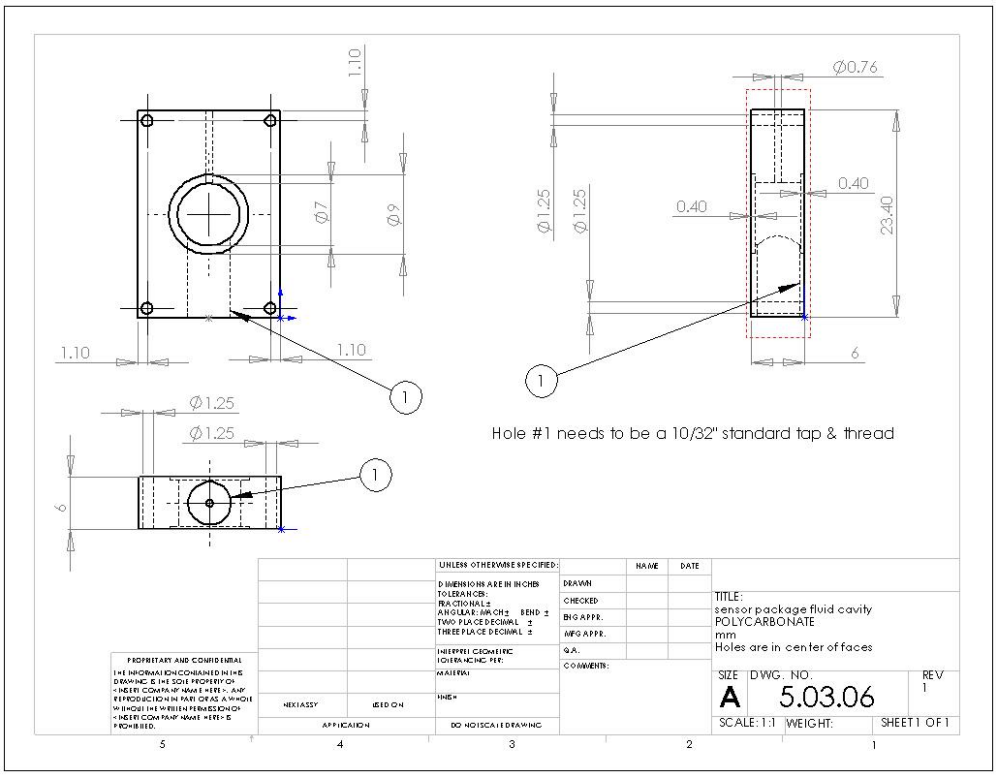

APPENDIX V.

MECHANICAL DRAWINGS FOR TYPE II PACKAGE TEST JIG.

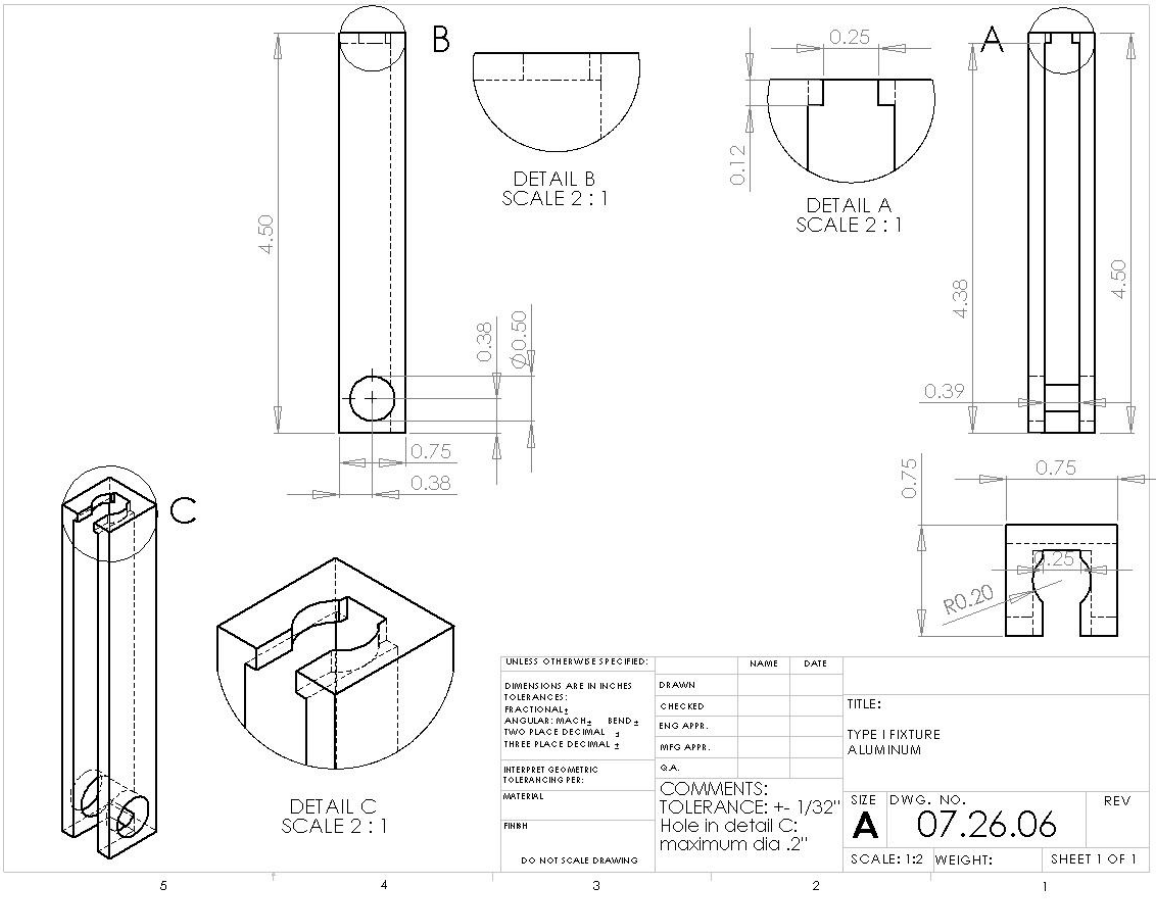

LIST OF REFERENCES

1. Janelle Anderson, D.T.C., Rebecca J. Jackman, Oksana Cherniavskaya, J. Cooper McDonald, Hongkai Wu, Sue H. Whitesides, and George M. Whitesides, *Fabrication of Topologically ComplexThree-Dimensional Microfluidic Systems in PDMS by Rapid Prototyping.* Analytical Chemistry, 2000. **72**(14): p. 3158-3164.
2. Bernhard T. Weigl, R.B., Thomas Schulte, Fred Batrell, and Jon Hayenga, *Design and Rapid Prototyping of Thin Film Laminate-Based Microfluidic Devices.* Biomedical Devices, 2001. **3**(4): p. 267-274.
3. Indalesio Rodriguez, P.S.-M., Christopher L. Kuyper, Gina S. Fiorini, Daniel T. Chiu, *Rapid prototyping of glass microchannels.* Analytica Chimica Acta, 2003(496): p. 205-215.
4. Papautsky, J.N.a.I., *Polymer embossing tools for rapid prototyping of plastic microfluidic devices.* JOURNAL OF MICROMECHANICS AND MICROENGINEERING, 2003. **14**: p. 96-103.
5. C. Gonzalez, S.D.C., R. L. Smith, *Fluidic interconnects for modular assembly of chemical microsystems.* SENSORS AND ACTUATORS B, 1998. **49**: p. 40-45.
6. Lin, J.-H.T.a.L., *Micro-to-macro Fluidic Interconnectors with an Integrated Polymer Sealant.* JOURNAL OF MICROMECHANICS AND MICROENGINEERING, 2001. **11**: p. 577-581.
7. B. L. Gray, S.D.C., R. L. Smith, *Interlocking mechanical and fluidic interconnections for microfluidic circuit boards.* SENSORS AND ACTUATORS A, 2004. **112**: p. 18-24.
8. Eunice S. Lee, D.H., Enzhu Liang, Scott D. Collins and Rosemary L. Smith, *Removable tubing interconnects for glass-based micro-fluidic systems made using ECDM.* JOURNAL OF MICROMECHANICS AND MICROENGINEERING, 2004. **14**: p. 535-541.
9. Pattekar, A.V. and M.V. Kothare, *Novel microfluidic interconnectors for high temperature and pressure applications.* Journal of Micromechanics and Microengineering, 2003. **13**(2): p. 337-345.
10. Puntambekar, A. and C.H. Ahn, *Self-aligning microfluidic interconnects for glass- and plastic-based microfluidic systems.* Journal of Micromechanics and Microengineering, 2001. **12**: p. 35-40.
11. Jaeggi, D., et al., *Novel Interconnection Technologies for Integrated Microfluidic Systems.* Proc. Solid State Sensor and Actuator Workshop, 1998: p. 112-115.
12. Peles, Y., et al., *Fluidic Packaging of Microengine and Microrocket Devices for High-Pressure and High-Temperature Operation.* J. Microelectromechanical Systems. **13**(1): p. 31-40.
13. Lee, E.S., et al., *Removable tubing interconnects for glass-based micro-fluidic systems made using ECDM.* Journal of Micromechanics and Microengineering, 2004. **14**: p. 535-541.
14. Yao, T.-J., et al., *Micromachined Rubber O-ring Micro-Fluidic Couplers.* IEEE Micro Electro Mechanical Systems, 2000: p. 624-627.
15. Pan, T., A. Baldi, and B. Ziaie, *A reworkable adhesive-free interconnection technology for microfluidic systems.* J. Microelectromechanical Systems, 2006. **15**(1): p. 267-272.

16. Gonzalez, C., S.D. Collins, and R. L. Smith, *Fluidic interconnects for modular assembly of chemical microsystems.* Sensors and Actuators B: Chemical, 1998. **49**: p. 40-45.
17. Gray, B.L., S.D. Collins, and R.L. Smith, *Interlocking Mechanical and Fluidic Interconnections for Microfluidic Circuit Boards.* Sensors and Actuators A: Physical, 2004. **112**: p. 18-24.
18. Enikov, E.T. and J.G. Boyd, *Electroplated electro-fluidic interconnects for chemical sensors.* Sensors and Actuators A: Physical, 2000. **84**: p. 161-164.
19. Han, A., et al., *A multi-layer plastic packaging technology for miniaturized bioanalysis systems containing integrated electrical and mechanical functionality.* Proc. 2nd Annual International IEEE-EMB Special Topic Conference on Microtechnologies in Medicine & Biology, 2002: p. 66-70.
20. Lawes, Z.C.a.R.A., *LOW COST FABRICATION OF MICROMECHANICAL SYSTEMS.* MICROELECTRONIC ENGINEERING, 1997. **35**: p. 389-392.
21. Fan-Gang Tseng, C.-S.Y., *High aspect ratio ultrathick micro-stencil by JSR THB-430N negative UV photoresist.* SENSORS AND ACTUATORS A, 2001. **97-98**: p. 764-770.
22. Ahmed Nadeem, M.M., Keith Rebello, Lee E. Weiss, Clarence Wu, Marc Feldman, and Michael L. Reed, *Fabrication of Microstructures Using Aluminum Anodization Techniques.*
23. S. Z. Chu, K.W., S. Inoue, and S. Todoroki, *Formation and Microstructures of Anodic Alumina Films from Aluminum Sputtered on Glass Substrate.* Journal of the electrochemical Society, 2002. **149**(7): p. B321-B327.
24. M. T.Wu, I.C.L., and M. H. Hon, *Growth characteristics of oxide during prolonged anodization of aluminum in preparing ordered nanopore.* Journal Vacuum Science and Technology, 2004. **22**(5).
25. R. Huang, K.R.H., and L. S. Chumbley, *Microscopic Observations of Voids in Anodic Oxide Films on Aluminum.* Journal of the electrochemical Society, 2004. **151**(7): p. B379-B386.
26. Xiaowei Zhao, P.J., Sishen Xie, Lifeng Liu, Weiya Zhou, Yan Gao, Li Song Jianxiong Wang, Dongfang Liu, Xinyuan Dou,Shudong Luo, Zengxing Zhang, Yanjuan Xiang, and Gang Wang, *Anodizing Behavior of Aluminum Foil Patterned with SiO_2 Mask.* Journal of the electrochemical Society, 2005. **152**(10): p. B441-B414.
27. N. PALSANDRAM, "*INTERCONNECTION, INTERFACE, AND INSTRUMENTATION FOR MICROMACHINED CHEMICAL SENSORS*," M.S. thesis, University of Central Florida, Orlando, Fl, 2005.
28. Tingrui Pan, A.B., and Babak Ziaie, *A Reworkable Adhesive-Free Interconnection Technology for Microfluidic Systems.* JOURNAL OF MICROELECTROMECHANICAL SYSTEMS, 2006. **15**(1): p. 267-272.
29. J Carlier, S.A., V Thomy, J C Fourier, F Caron, J C Camart, C Druron and P tabourier, *Integrated microfluidics based on multi-layered SU-8 for mass spectrmetry analysis.* JOURNAL OF MICROMECHANICS AND MICROENGINEERING, 2004. **14**: p. 619-624.
30. C. R. Tamanaha, l.j.w., and r j. colton, *hybrid macro-micro fluidics system for a chip-based biosensor.* JOURNAL OF MICROMECHANICS AND MICROENGINEERING, 2002. **12**: p. n7-n17.

31. Fries, J.S.a.D., *Rapid Prototyping and Development of Microfluidic and BioMEMS Devices*, in *IVD Technology*, R. Grace, Editor. 2002.
32. Tang, Y., *STEREOLITHOGRAPHY CURE PROCESS MODELING*, in *CHEMICAL & BIOMOLECULAR ENGINEERING*. 2005, Georgia Institute of Technology. p. 177.
33. Lawes, R.A., *Manufacturing tolerances for UV-LIGA using SU-8.* JOURNAL OF MICROMECHANICS AND MICROENGINEERING, 2005. **15**: p. 2198-2203.
34. Dapeng Zhu, L.W., YingjunCheng, Gaowei Xu, Le Luo. *Studies on fabrication of high density MCM-D substrate by aluminum anodization techniques*. in *6th International Conference onElectrnic Packaging Technology*. 2005: IEEE.
35. ER. Huang, K.R.H., and L. S. Chumbley, *Microscopic Observations of Voids in Anodic Oxide Films on Aluminum.* Journal of the electrochemical Society, 2004. **151**(7): p. B379-B386.
36. R. W. Stark, M.S.S., A. Stemmer, *Microfluidic etching driven by capillary forces for rapid prototyping of gold stuctures.* MICROELECTRONIC ENGINEERING, 2003. **67-68**: p. 229-236.
37. Miniature, C.i., *THE LCD ANODIZING SYSTEM.* 2003.
38. Seong-Hyok Kim, S.-H.L.a.Y.-K.K., *A high-aspec-ration comb actuator using UV-LIGA surface micromachining and (110) silicon bulk micromachining.* JOURNAL OF MICROMECHANICS AND MICROENGINEERING, 2002. **12**: p. 128-135.
39. Moore, E.H.C.a.D.F., *SU-8 thick photoresist as a functional material for MEMS Applications.* JOURNAL OF MICROMECHANICS AND MICROENGINEERING, 2002. **12**: p. 368-374.
40. J Zhang, K.L.T., G D Hong, L J Yang and H Q Gong, *Polymerization optimization of SU-8 photoresist and its applications in microfluidic systems and MEMS.* JOURNAL OF MICROMECHANICS AND MICROENGINEERING, 2001. **11**: p. 20-26.
41. Madou, M.J., *Fundamentals of Microfabrication*. 2nd edition ed. 1997, Boca Raton: CRC Press LLC.
42. M. Goretty, A.A., *Polymer Microfabrication for Microarrays, Microreactors, and Microfluidics.*
43. Thayne L. Edwards, S.K.M., Russel K. Edwards, Charles Thomas, A. Bruno Frazier, *RAPID TOOLING USING UV-LIGA FOR INJECTION MOLDING MICROFLUIDIC COMPONENTS*, Georgia Institute of Technology and University of Utah.
44. Matthew Hopcroft, T.K., Gyuman Kim, Kazuki Takashima, Yakichi Higo, David Moore and Jueren Brugger, *Micromechanical testing of SU-8 cantilevers.* JSME-MMD, 2003.
45. Hwa Seng Khoo, K.-K.L.a.F.-G.T., *Mechanical strength and interfacial failure analysis of cantilevered SU-8 micrposts.* JOURNAL OF MICROMECHANICS AND MICROENGINEERING, 2003. **13**: p. 822-831.